Ceres's global and localized mineralogical composition determined by Dawn's Visible and Infrared Spectrometer (VIR)

M. C. De SANCTIS [1*], E. AMMANNITO[2], F. G. CARROZZO[1], M. CIARNIELLO[1],
M. GIARDINO[1], A. FRIGERI[1], S. FONTE[1], H. Y. McSWEEN [3], A. RAPONI[1], F. TOSI [1],
F. ZAMBON[1], C. A. RAYMOND[4], and C. T. RUSSELL[5]

[1]Istituto di Astrofisica e Planetologia Spaziali, INAF, Rome, Italy
[2]Agenzia Spaziale Italiana, Rome, Italy
[3]Department of Earth & Planetary Sciences and Planetary Science Institute, University of Tennessee, Knoxville, Tennessee
37996–1410, USA
[4]Jet Propulsion Laboratory, Pasadena, California 91109, USA
[5]Institute of Geophysics and Planetary Physics, University of California, Los Angeles, California 90095–1567, USA
[*]Corresponding author. E-mail: mariacristina.desanctis@iaps.inaf.it

Abstract–The Visible and Infrared Spectrometer (VIR) instrument on the Dawn mission observed Ceres's surface at different spatial resolutions, revealing a nearly uniform global distribution of surface mineralogy. Clearly, Ceres experienced extensive water-related processes and chemical differentiation. The surface is mainly composed of a dark component (carbon, magnetite?), Mg-phyllosilicates, ammoniated clays, carbonates, and salts. The observed species suggest endogenous, global-scale aqueous alteration. While mostly uniform at regional scale, Ceres's surface shows small localized areas with different species and/or variations in abundances. Few local exposures of water ice are seen, especially at higher latitudes. Sodium carbonates have been identified in several areas on the surface, notably in Occator bright faculae. Organic matter has also been discovered in several places, most conspicuously in a large area close to the Ernutet crater. The observed mineralogies, with the presence of ammoniated species and sodium salts, have a strong resemblance to materials found on other bodies of the outer solar system, such as Enceladus. This poses some questions about the original material from which Ceres accreted, suggesting a colder environment for such material with respect to Ceres's present position.

PREVIOUS STUDIES OF CERES'S MINERALOGY

The Dawn mission was launched in September 2007 to study the two most massive bodies in the asteroid belt: the asteroid Vesta and the dwarf planet Ceres. The spacecraft is equipped with a suite of three instruments: a Visible and Infrared Spectrometer (VIR) (De Sanctis et al. 2011), two redundant Framing Cameras (FCs) (Sierks et al. 2011), and a Gamma Ray and Neutron Detector (GRaND) (Prettyman et al. 2011). Moreover, gravity data are retrieved via tracking with the radio communication system. The Dawn spacecraft permitted detailed study of Ceres's surface by VIR and, together with the other instruments, confirmed that Ceres has experienced pervasive aqueous alteration on a planetary scale (Russell et al. 2016).

Before Dawn's arrival in 2015, our knowledge of Ceres's composition was derived from ground-based and space-based telescopic data (McCord and Castillo Rogez 2018). In recent years, Ceres has been the subject of increased attention from the community (e.g., Thomas et al. 2005; Li et al. 2006; Rivkin et al. 2006a, 2006b; Milliken and Rivkin 2009; Rousselot et al. 2011). Disk-resolved imaging of Ceres has allowed determination of its size, shape, spin, and density (Thomas et al. 2005; Carry et al. 2008). Many high-quality color data and spectra of Ceres have been acquired using Earth-based telescopes.

Ceres has long been associated with the carbonaceous chondrites based on its albedo and visible/near-IR (0.4–2.5 μm) spectrum. In fact, the spectra are often "flat" in that range. Also, Ceres's spectrum is relatively flat without recognizable spectral features in that spectral range, so the identification of the mineral constituents of the surface was not easy. The wavelength range beyond 2.5 μm hosts many absorptions, including those due to water, hydroxyl, organic matter, carbonates, carbon dioxide, ammonia, and other volatiles. Thus, this spectral range is more suitable for understanding Ceres's composition and surface mineralogy. Unfortunately, the spectral region between 2.6 and 2.9 μm is not accessible from the ground due to atmospheric water absorption, which has limited our knowledge of the near-IR Ceres's spectrum.

The most obvious features of Ceres's spectrum between 2.5 and 4 μm from the ground are a relatively narrow absorption band centered near 3.06 μm and sets of overlapping bands from 3.3 to 3.4 μm and 3.8 to 3.9 μm. The band at 3.06 μm, very unusual among solar system bodies, was first interpreted to indicate a very thin water ice frost (Lebofsky 1978; Lebofsky et al. 1981) and was later re-interpreted as due to NH_4-bearing phyllosilicates (King et al. 1992). More recently, Vernazza et al. (2005) suggested a mixture of irradiated organics and crystalline water ice as responsible for the 3.06 μm band. Rivkin et al. (2006a, 2006b) interpreted the 3.06 μm band as due to an iron-rich clay and the 3.3–3.4 and 3.8–3.9 μm bands to be produced by carbonates, but the same absorptions were re-interpreted by Milliken and Rivkin (2009) as brucite ($Mg(OH)_2$) and carbonates.

Ground-based and HST images of Ceres revealed that the surface is mostly uniform and exhibits very small color and albedo variations. The surface albedo variation is ~6% with respect to the average value, with possible broad-band color variations of ~2–3% and small variations (~2%) of the spectral slope (Li et al. 2006; Carry et al. 2008). They are broadly correlated with the albedo variations indicated by the HST and Keck data of Ceres (Li et al. 2006; Carry et al. 2008).

Rotationally resolved near-infrared spectra of Ceres were acquired by Rivkin and Volquardsen (2009), who reported evidence for a relatively uniform surface. Recently, Kueppers et al. (2014) identified water vapor from two localized sources on Ceres, suggesting that water outgassing was due to comet-like sublimation or cryovolcanism. Previously, the presence of water vapor around Ceres was suggested by a marginal detection of hydroxyl (A'Hearn and Feldman 1992), but the emission was not confirmed by later observations (Rousselot et al. 2011).

DAWN AT CERES

Dawn's instrument suite was designed to characterize several aspects of the physical properties and composition of Vesta and Ceres. Dawn was planned as a mapping mission with different phases at decreasing distance from the bodies' surfaces (Russell and Raymond 2011). Specifically at Ceres, the Dawn's orbital phases were as follows: Approach phase (CSA), starting at 382,360 km from the surface and continuing to 22,406 km; Rotational characterization (CSR) at a distance of 13,591 km; Transfer orbit (CST) at 6187 km; Survey orbit at ~4397 km altitude; High Altitude Mapping Orbit (HAMO) at 1459 km altitude; Low Altitude Mapping Orbit (LAMO) at 376 km altitude; and four Extended phases: from XM001 (eXtended Mission 001) at 382 km altitude; XM002 at 1491 km; XM003 at 7594 km, and the last XM004 at 19,436 km. The HAMO orbits were performed in two different periods: HAMO in autumn 2015 between Survey and LAMO, and Extended HAMO (XM002—eXtended Mission 002) in autumn 2016 after LAMO.

The VIR Instrument

The VIR (De Sanctis et al. 2011) is an imaging spectrometer operating between 0.25 and 5.1 μm, a range that contains diagnostic mineral absorption bands as well as the 3 μm "water" region. The VIR experiment is derived from VIRTIS-M aboard Rosetta and Venus Express (Reininger et al. 1996; Coradini et al. 1998); all these instruments are based on the optical layout of the Cassini/VIMS-V. VIR shares a Shafer telescope and an Offner relay between two spectral channels: the VIS channel operates in the 0.25–1.05 μm range, while the IR operates between 1.0 and 5.0 μm. The high spatial (IFOV = 250 μrad/pixel, FOV = 64 × 64 mrad) and spectral (ΔλVIS = 1.8 nm/band; ΔλIR = 9.8 nm/band) performances allow for the identification and mapping of compositional units on the surfaces.

Images are acquired using a scanning mirror or using the S/C movement with respect to the body surface: the scene is scanned one line at a time through the entrance slit of the spectrometer. Each line is made up of several pixels, each having a spectrum in the overall 0.25–5.1 μm range. The set of adjacent images is then stacked to form a "cube." Thus, it is possible to extract a spectrum from each pixel in the data cube, showing the intensity of light as a function of the wavelength for that specific pixel. At the same time, it is possible to extract monochromatic images of the entire scene for a specific wavelength. Each pixel represents the radiance measured at a location on the ground; part

Table 1. Data acquired by VIR during the different mission phases.

Start date	Phase	Nominal resolution (m/px)	Distance from surface (km)	No. of spectra IR	No. of spectra VIS
2015-01-13	CSA (Ceres Science Approach)	95,590–5601	382,360–22,406	1,585,664	1,585,664
2015-04-25	CSR (Ceres Science Rotation Characterization)	3398	13,591	1,958,400	1,958,400
2015-05-16	CTS (Ceres Transfer to Survey)	1547	6187	193,536	193,536
2015-06-05	CSS (Ceres Science Survey)	1099	4397	2,890,240	4,339,968
2015-08-18	CSH (Ceres Science High Altitude Mapping Orbit)	365	1459	9,132,032	3,494,400
2015-12-16	CSL (Ceres Science Low Altitude Mapping Orbit)	94	376	11,343,616	10,432,000
2016-08-12	XM01 (eXtended Mission 001)	96	382	230,400	1,792,000
2016-10-17	XM02 (eXtended Mission 002)	373	1491	569,088	0
2017-01-27	XM03 (eXtended Mission 003)	1899	7594	0	58
2017-04-29	XM04 (eXtended Mission 004)	4859	19,436	9728	228,608

of the radiance is reflected sunlight, but at longer wavelengths, it also includes thermally emitted radiance and not only reflected light.

VIR Ceres Observations and Data Reduction

The VIR acquired data for Ceres during all of the mission phases, from Approach through the Extended Mission, during more than 2 yr of operations. The total number of spectra collected at Ceres, sampled in 864 spectral channels from 0.25 to 5.1 μm, exceeds 50 million, with variable spatial resolutions. Ceres's surface was mapped with increasing spatial resolution from Survey (CSS) to LAMO orbits (CSL), but this increase was at the expense of coverage. Table 1 summarizes data acquired during the different mission phases, and Fig. 1 shows the coverage during Survey, HAMO, and LAMO.

The data were calibrated and processed to analyze them in terms of overall Ceres mineralogy. The calibration file has been improved with respect to Vesta published data in which a calibration artifact was present in the region between 2.5 and 3 μm. Both the flat field and the spectral response are improved in this new calibration (Carrozzo et al. 2016). More information is given in Appendix 1.

Ceres spectra are affected by thermal emissions from ~3.2 μm longward, and we implemented an algorithm to remove the thermal emission. This is made by modeling the total radiance as the sum of the solar radiance reflected by the surface and the thermal emission of the surface itself, and then performing the removal of the latter, as fully described in Raponi et al. (2017a). The main difference, with respect to a simple fitting of a Planck function, is the modeling of the reflectance of the surface, multiplied by the solar

irradiance at Ceres's heliocentric distance. With this approach, we used the same reflectance model to estimate the reflectance level in the thermal emission range, then the Planck function is summed to this model to fit the total radiance level of the spectrum. After the estimation of the Planck function, we subtract it from the total measured radiance, and we divide the result by the solar irradiance to obtain the reflectance in the whole range (see Raponi et al. [2017a] for further details).

Here, we describe the main results obtained by analyzing the spectra of different regions of Ceres, as well as the average Cerean composition.

CERES SPECTRAL CHARACTERISTICS

Ceres Global Spectra

The average thermally corrected reflectance spectrum of Ceres (Fig. 2) is almost flat in the spectral region below 2.6 μm, with the exception of a broad inflection at about 1.2 μm, possibly due to Fe. However, a broad and very shallow band is visible in the VIS spectral region at about 0.75 μm, which is still under evaluation, due to the low S/N in the VIS range.

The spectrum shows that the 2.6–4.2 μm wavelength region is characterized by a broad asymmetric feature (Fig. 2C), in which several distinct absorptions appear at 2.72, 3.05–3.1, 3.3–3.5, and 3.95 μm. The most prominent is a strong and narrow absorption centered at 2.72–2.73 μm, which was not visible from the ground due to the telluric absorption.

The absorption feature at 2.72–2.73 μm is typical of OH-bearing minerals; H_2O-bearing phases have a much broader absorption band that does not fit the Ceres spectrum. The other absorptions are attributed to
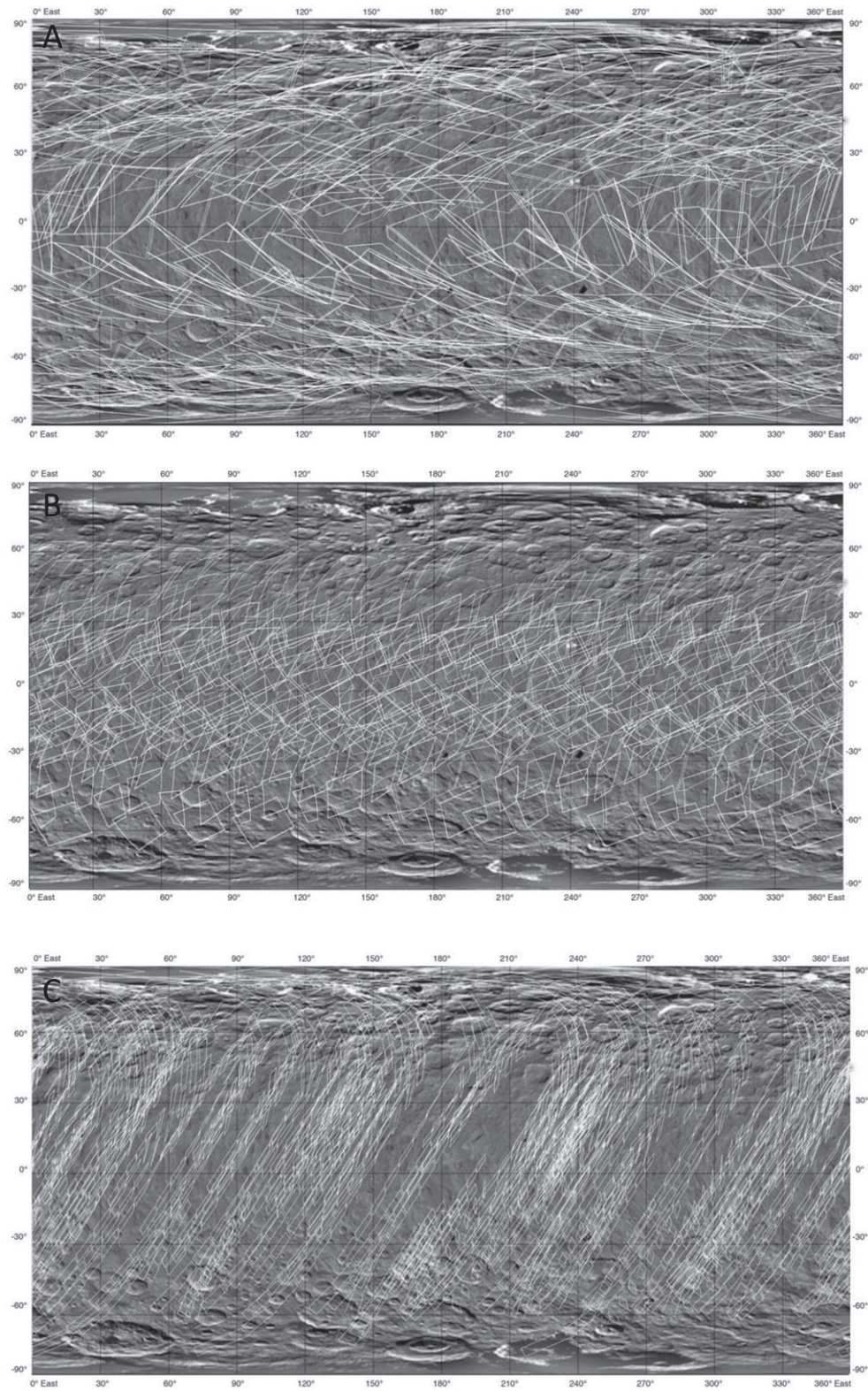
Fig. 1. Coverage and distribution of the VIR cubes acquired during (a) CSS and CTS, (b) HAMO, (c) LAMO orbital phases. The background image is a cylindrical projection mosaic of FC clear-filter data (credit: NASA/JPL-Caltech/UCLA/MPS/DLR/IDA).
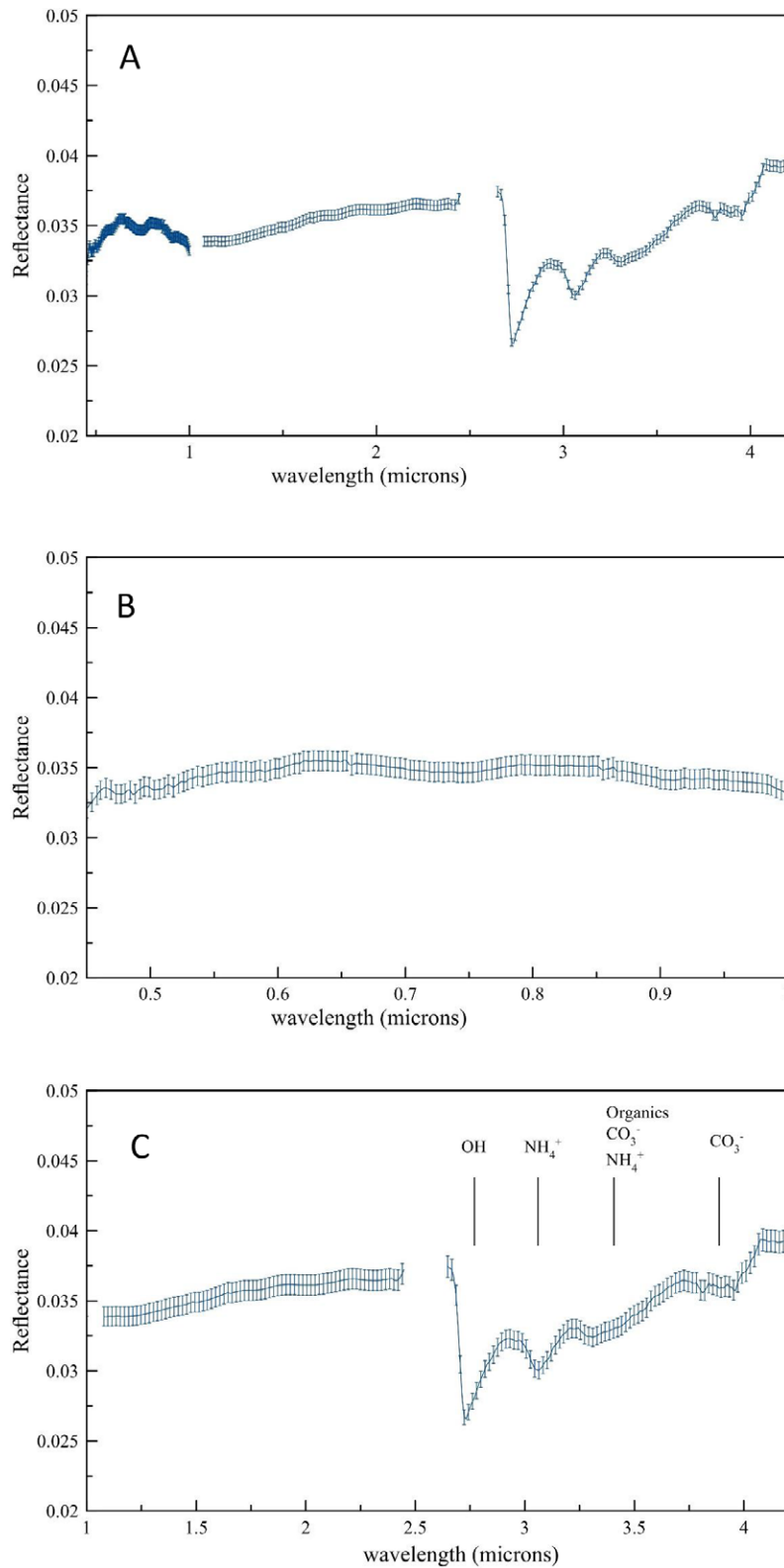
Fig. 2. Ceres average spectrum: (A) thermally corrected average spectrum of Ceres in the spectral range 0.4–4.2 μm, (B) average spectrum of Ceres in the spectral range 0.4–1 μm, (C) average spectrum of Ceres in the spectral range 1–4.2 μm. The spectrum has been computed using the photometric parameters as derived by Ciarniello et al. (2017) using the Hapke model. The spectrum is computed for incidence angle = 30° and emission angle = 0°. (Color figure can be viewed at wileyonlinelibrary.com.)

carbonate (~3.9 µm) and ammoniated phyllosilicates (3.06 µm). The 3.06 µm band has been attributed to several other chemical species in the past, as previously noted. The broad signature between 3.3 and 3.6 µm can be the result of overlapping absorptions due to carbonates, ammoniated phyllosilicates, and organics (Moroz et al. 1998; Beran 2002; Bishop et al. 2008). Comparison between the Ceres OH-band and those of terrestrial phyllosilicates (Fig. 3) indicates the presence of Mg-OH phases, such as antigorite (Mg-serpentine) or saponite (Mg-smectite). In fact, OH-stretching vibrations that occur in the 2.7–2.85 µm range for phyllosilicates have band centers at different wavelengths for different species (Farmer 1974; King and Clark 1989; Beran 2002; Bishop et al. 2008) (Table 2). In Table 3, the names of the laboratory spectra used in the following figures are reported.

The band at 3.06 µm has been interpreted in different ways in the last few years, but the best match, also taking into consideration the overall spectrum, is ammoniated phyllosilicates (Fig. 4). Laboratory spectra of ammoniated phyllosilicates show narrow bands near 3.05–3.07 µm, broad complex bands at 3.25–3.30 µm (assigned to NH_4^+ species in the samples), and also a small feature near 3.50–3.55 µm (Bishop et al. 2002). All these features are present in Ceres's average spectrum.

The signatures at 3.9 and 3.4–3.5 µm have been assigned to carbonates. Different carbonates have signatures with band centers in different positions. By comparing the Ceres signature with the carbonate absorptions, it is possible to identify the predominant carbonate present (Fig. 5). The best match is with dolomite or magnesite (De Sanctis et al. 2015). All the minerals identified from absorptions in the IR range have relatively high albedo, while the geometric albedo of Ceres is about 0.08 (Ciarniello et al. 2017), spectrally dominated by a dark, highly absorbing component. This material is spectrally featureless and is, therefore, difficult to constrain. It could be a dark phase like magnetite or carbon. Thus, the overall spectrum of Ceres is best fitted with a mixture of dark material, Mg-phyllosilicates, ammoniated phyllosilicates, and carbonates (De Sanctis et al. 2015).

Comparison with Meteorites

Carbonaceous chondrites have often been considered as spectral analogs for the surface of Ceres. In fact, the low reflectance and some absorptions in the IR are good matches for part of the Ceres spectrum. Among the carbonaceous chondrites, the CM and CI classes are widely thought to derive from the C-complex asteroids and are plausible analogs for Ceres (McSween
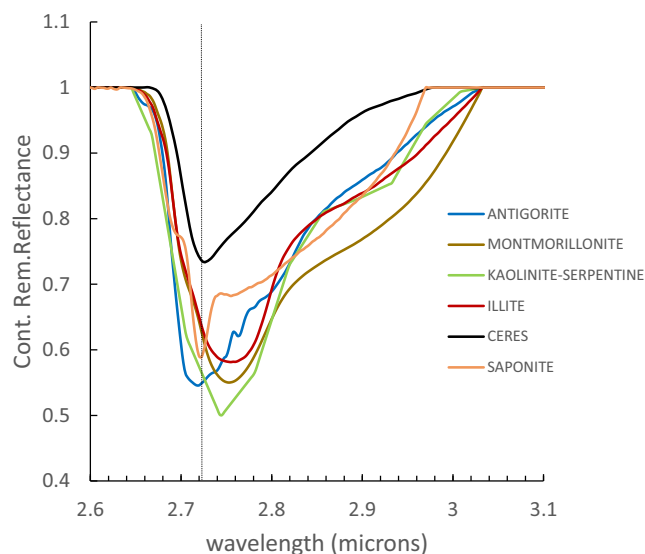

Fig. 3. Comparisons between the OH-absorption feature at 2.7 µm of Ceres with those of some terrestrial phyllosilicates. The spectra of terrestrial phyllosilicates have been multiplied for a dark neutral component to make the comparison easier. (Color figure can be viewed at wileyonlinelibrary.com.)

Table 2. OH band centers for phyllosilicates.

	Wavelengths (microns)	Reference
Montmorillonite	~2.75	Bishop et al. (2008)
Fe-smectite	~2.75, ~2.8	Bishop et al. (2008)
Mg-smectite	2.72	Bishop et al. (2008)
Nontronite	2.80	Bishop et al. (2008)
Kaolinite	2.71, 2.73, 2.74, 2.76	Bishop et al. (2008)
Muscovite	2.76	Beran (2002)
Chrysotile	2.71, 2.74,	Bishop et al. (2008)
Phlogopite	2.69	Beran (2002)

et al. 2017). A laboratory characterization of spectra of selected CM and CI chondrites (Takir et al. 2013) found a relation between petrologic and geochemical parameters and spectral properties. A comparison between Ceres average spectrum and CI/CM spectra indicates that the 2.7 µm phyllosilicate band and the carbonate band are similar to those of some CIs, but the other bands are not fully represented in CM and CI spectra (Fig. 6).

The phyllosilicate band dominates the spectra of CM and CI chondrites, while the carbonate band is barely visible. The organic band is stronger in the meteorites' spectra with respect to Ceres, but the organic band could also be due to terrestrial contamination of the samples. According to Takir et al. (2013), the 3 µm band center decreases with increasing alteration of the chondrites and the most altered chondrites have 3 µm band centers at shorter wavelength, consistent with Mg-rich serpentine and smectite minerals. The CM

Table 3. Spectra used in Figs. 3–5 and in the spectral fits.

|		
Brucite	JB-JLB-944	Janice L. Bishop, SETI Institute
Illite	LAIL03	CRISM Spectral Library
Smectite	BKR1JB013	CRISM Spectral Library
Antigorite (1)	LAAT02	CRISM Spectral Library
Antigorite (2)	AT-TXH-006	T.X. Hiroi RELAB Spectral Library
Montmorillonite	LAMO02	CRISM Spectral Library
NH$_4$-montmorillonite	JB-JLB-189	Janice L. Bishop, SETI Institute
NH$_4$-annite	AA-A1S-002	Alexander Smirnov, State University of New York, Dept. of Geosciences
Dolomite (1)	F1CC05B	CRISM Spectral Library
Dolomite (2)	CB-EAC-003	E.A. Cloutis RELAB Spectral Library
Calcite	LACB10A	CRISM Spectral Library
Siderite	LACB08B	CRISM Spectral Library
Ankerite	LACB01B	CRISM Spectral Library
Aragonite	KACB02B	CRISM Spectral Library
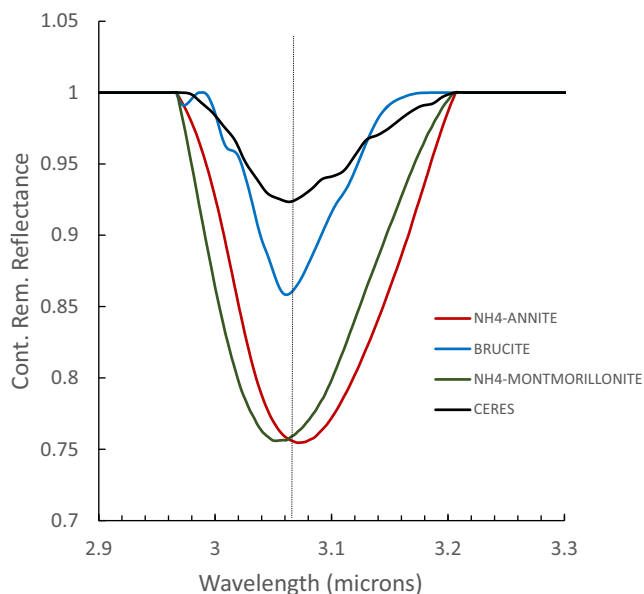
Fig. 4. Comparisons between the absorption feature at 3.07 μm of Ceres with those of brucite and ammoniated clays. The spectra of laboratory samples have been multiplied for a dark neutral component to make the comparison easier. (Color figure can be viewed at wileyonlinelibrary.com.)

and CI meteorites are classified according to their degree of alteration: (1) the less altered chondrites are characterized by phyllosilicate band centers at 2.76–2.80 μm, consistent with the Fe-serpentine (cron-stedtite); (2) those with an intermediate degree of alteration have band centers at 2.76–2.78 μm; (3) the most altered, which are characterized by band centers at ~2.72 μm, are consistent with Mg-serpentine (antigorite). The Ceres phyllosilicate band center is similar to those of the most altered CMs, indicating a very high degree of aqueous alteration (McSween et al. 2017, this issue).

The most striking difference between the Ceres spectrum and the CM and CI spectra is the presence of the 3.07 band in Ceres, attributed to ammoniated phyllosilicates. Ammoniated phyllosilicates have not been detected in carbonaceous chondrites, but NH$_3$ is a component of organic matter in CM, CI, and CR chondrites (Pizzarello and Williams 2012). Experiments indicate that the ammonia in carbonaceous chondrites is released upon heating of the samples at 300 °C (Pizzarello and Williams 2012). In contact with liquid water, NH$_3$ forms NH$_4^+$, which could exchange with cations in clays forming NH$_4$-phyllosilicate. However, if this is the case, we might expect to also see this kind of ammoniated species in the most altered meteorites that share the same kind of phyllosilicate (Mg rich) with Ceres. The absence of this ammonia-rich mineralogy among the CI, CM, and CR chondrites is indicative of processes different from the hydrothermal alteration acting on the CC parent bodies. Alternatively, the ammonia-rich clays are the result of a different initial composition of Ceres suggestive of a more volatile ice-rich and colder environment with respect to the main belt (De Sanctis et al. 2015).

OBSERVED MINERALOGIES

The global surface occurrence of dark material, Mg-phyllosilicates, ammoniated phyllosilicates, and (Mg, Ca)-carbonates is mostly uniform, and we do not observe any large km-sized areas that lack the above-mentioned species (Ammannito et al. 2016; Carrozzo et al. 2018). However, variations in the strength of the absorption features are spatially correlated and indicate considerable variability in the relative abundance of the phyllosilicates, although their compositions are fairly uniform. Also carbonates are ubiquitous, but they show local variations in composition and abundance (De Sanctis et al. 2016; Carrozzo et al. 2018). Ammonium-bearing minerals are widespread and ubiquitous on the surface of Ceres, even if they show a difference in abundances and in the chemical forms (Ammannito et al. 2016; De Sanctis et al. 2016). The described mineralogy requires pervasive and long-standing aqueous alteration (McCord and Castillo Rogez 2018) as also indicated by the high spatial uniformity of element abundance measurements of equatorial regolith
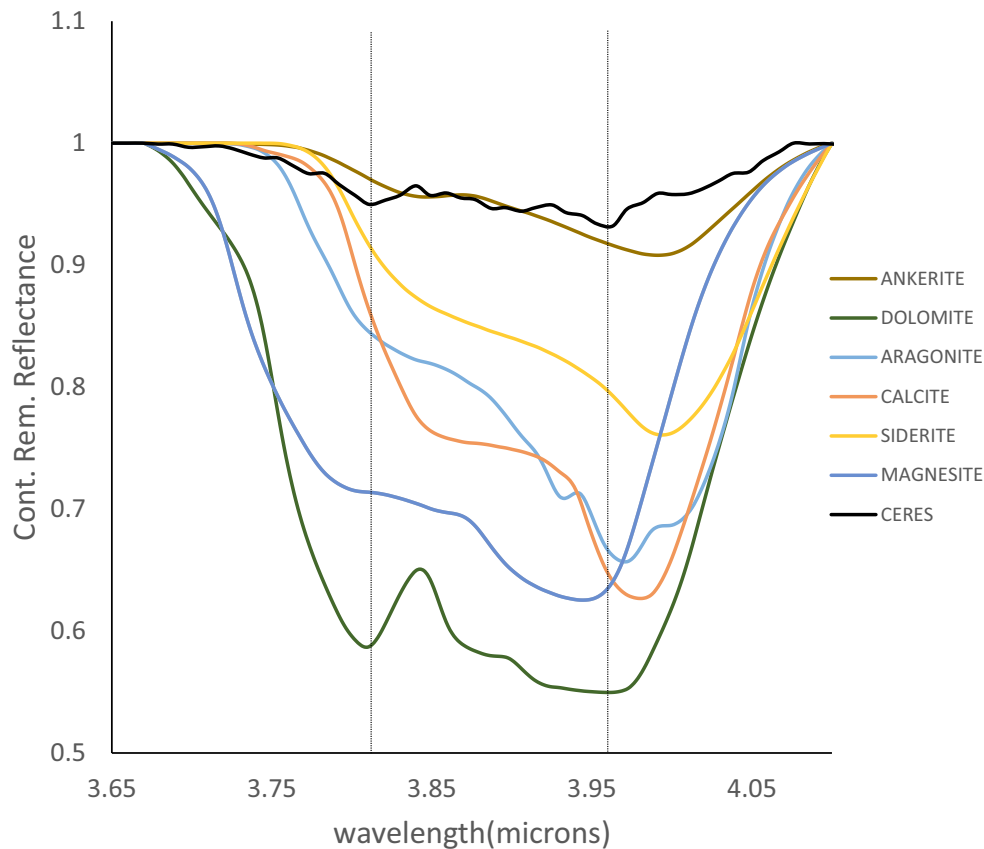
Fig. 5. Comparisons of the absorption feature at 3.9 μm of Ceres with those of terrestrial carbonates. The spectra of laboratory samples have been multiplied for a dark neutral component to make the comparison easier. (Color figure can be viewed at wileyonlinelibrary.com.)

(Prettyman et al. 2016); indeed, water ice has been identified on the surface of Ceres in a few localized small areas, such as the craters Oxo and Juling (Combe et al. 2016, 2017; De Sanctis et al. 2017a; Raponi et al. 2017b). Another interesting area is close to the Ernutet Crater, where the spectral signature of organics has been detected by VIR (De Sanctis et al. 2017b). Local sites having large exposures of different mineralogies are identified in Fig. 7.

Comparison of the thermal and chemical Ceres modeling results (Castillo et al. 2018) with observed surface mineralogy indicates advanced alteration under a relatively high fugacity of hydrogen, consistent with large ice-rich bodies. Simulations by Castillo et al. (2018) show that ammoniated clays and carbonates can both be produced under similar conditions. Moreover, two types of carbonates are found from the simulations: one type of carbonates, such as calcite, magnesite, or dolomite, precipitate with the altered rocks, due to their low solubilities at the conditions of interest. The other type (Na-rich) remains in solution and forms the precursor of sodium bicarbonate. Hence, the

simulations show that both Mg/Ca carbonate, observed across the surface (De Sanctis et al. 2015), and Na-carbonate, detected at the Occator bright spots (De Sanctis et al. 2016), originate under the same environmental conditions.

Phyllosilicates

The phyllosilicate band center is set at 2.72 μm for most of the observed portion of Ceres (Ammannito et al. 2016). However, very limited areas occur in which the phyllosilicate band shifts toward longer wavelengths, indicating a different chemical composition of the phyllosilicate. One example is the small bright central region of the Occator Crater floor, where a shift of the band at 2.78 μm is visible. A few bright pixels in the Kupalo Crater also show a shift to longer wavelengths (De Sanctis et al. 2017a). The shift of the phyllosilicate band is visible in the high spatial resolution data (~100 m/px). The shift of the metal-OH absorption from 2.72 μm to longer wavelengths (Fig. 8) indicates the additional occurrence of another phyllosilicate.
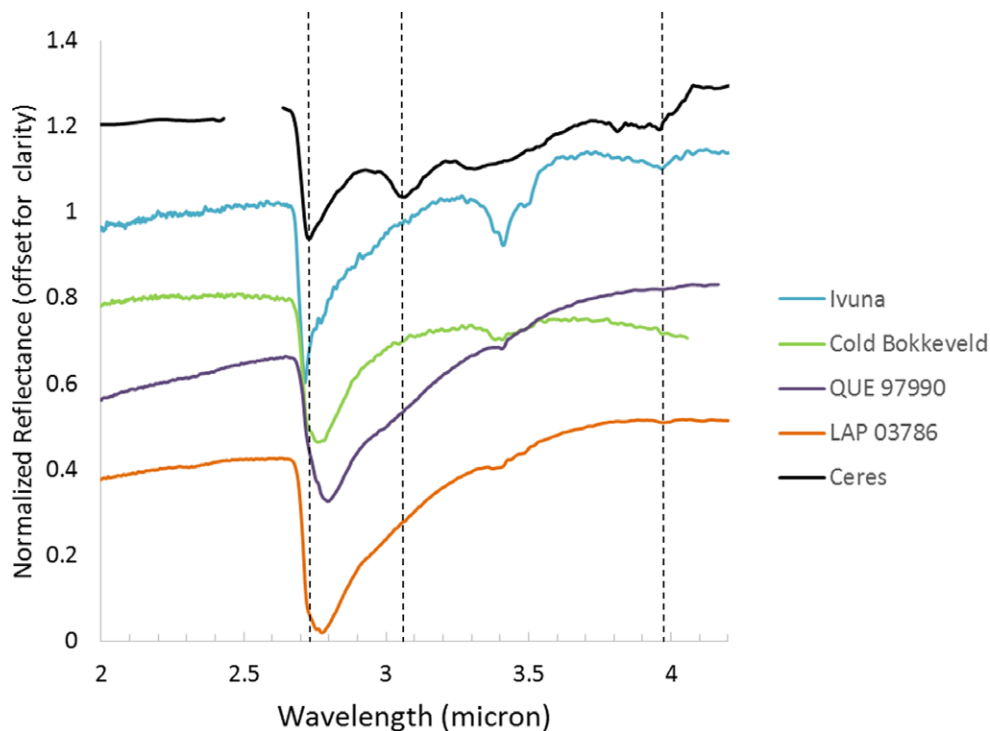
Fig. 6. Comparisons of Ceres average spectrum with IR reflectance spectra of CM and CI carbonaceous chondrites measured under dry and vacuum conditions (Takir et al. 2013). (Color figure can be viewed at wileyonlinelibrary.com.)
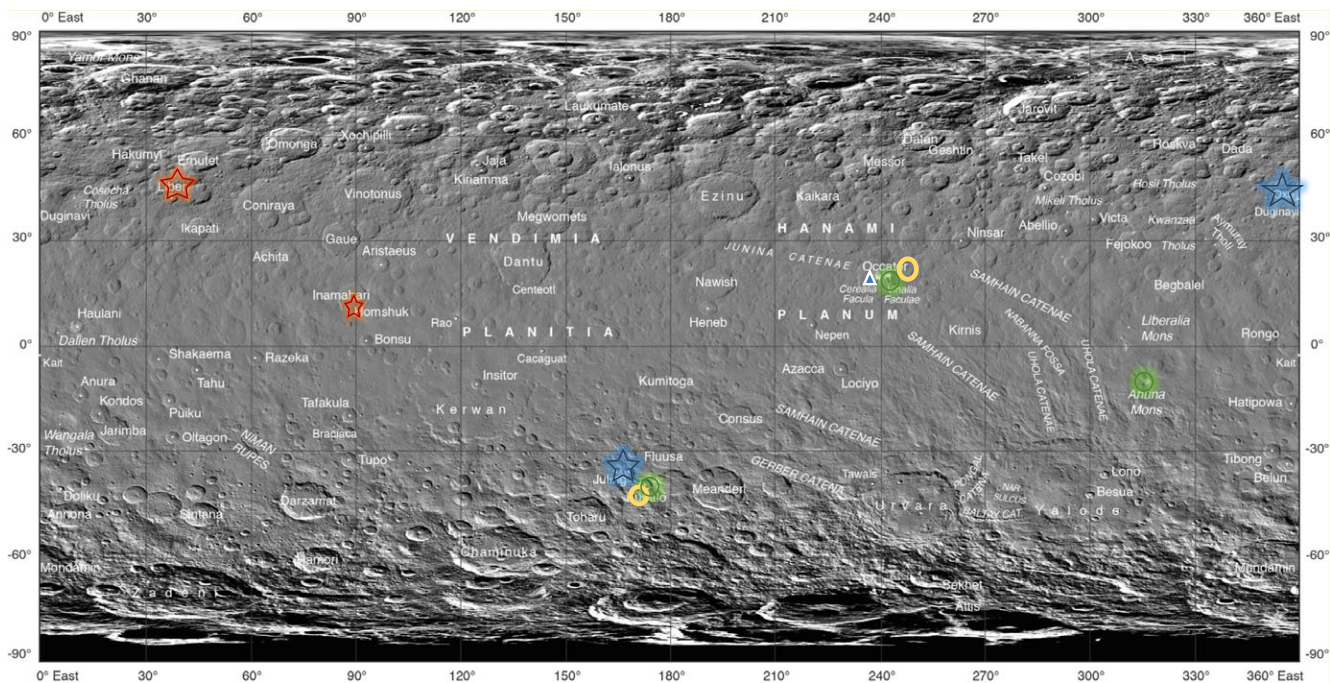

Fig. 7. Map of Ceres with highlighted locations where the localized mineralogies described in this section are found. Red stars indicate organic materials, blue stars indicate the major location where water ice was found, purple circles indicate Na-carbonates, yellow circles indicate different phyllosilicates, and the triangles indicate ammonium salts. The background image is a cylindrical projection mosaic of FC clear-filter data (credit: NASA/JPL-Caltech/UCLA/MPS/DLR/IDA). (Color figure can be viewed at wileyonlinelibrary.com.)

Typically, Mg-phyllosilicates show band absorptions at ~2.72–2.73 μm, whereas Al-phyllosilicates have absorptions at ~2.75–2.76 μm. This phase could possibly be smectite, kaolinite, or illite (Table 2). We cannot exclude other smaller areas having OH absorptions at longer wavelengths with respect to the average value.

Although the detected phyllosilicates are mostly compositionally homogeneous, the intensity of their absorption features at 2.7 μm varies (Ammannito et al. 2016). Such variations are likely due to spatial variability in relative mineral abundance.

Ammonium Species

Ceres's surface is characterized by an absorption band at ~3.07 μm, here interpreted as the presence of phyllosilicates bearing NH_4 from the Dawn data. The carrier of this band has been under debate since the first observation of Ceres in that spectral range, and initially interpreted as water ice (Lebofsky 1978; Lebofsky et al. 1981). Later studies suggested this band was due to the presence of hydrated clays or NH_4-bearing clays (Feierberg et al. 1981; King et al. 1992). More recently, brucite was considered to be the carrier of the 3.07 μm signature. However, due to the extended spectral range provided by VIR spectrometer on the Dawn mission, this band has been interpreted as due to the presence of ammoniated clays on the Ceres surface (De Sanctis et al. 2015).

In fact, spectral fits, using as endmembers both NH_4-phyllosilicates and brucite, to account for the 3.07 μm band, always give the best fit using a large amount of NH_4-phyllosilicates (Fig. 9) and a negligible amount of brucite. In the spectral fit reported in Fig. 9, brucite content is less than 1%, while ammoniated clays are about 9% of the mixture.

Forcing the fits to have only brucite in the mixture without ammoniated phyllosilicates results as unreasonable, as shown in Fig. 10, where we imposed 5% (Fig. 10A) and 10% (Fig. 10B) of brucite and 0% ammoniated clays (the endmembers used are reported in Table 3). In both cases, the presence of brucite is not sufficient to match the Ceres spectrum.

The precise identification of specific ammoniated phyllosilicate on Ceres is still under evaluation. In fact, some kinds of phyllosilicate, such as smectites, readily ammoniate, whereas serpentine and chlorite minerals do not (Bishop et al. 2002; Ehlmann et al. 2018). The ammonium cation resides in the interlayer sites of the sheet silicate structure as an exchangeable ion competing with Ca^{2+}, Mg^{2+}, Na^+, or K^+. In certain clays, such as illite and highly charged smectite, NH_4^+
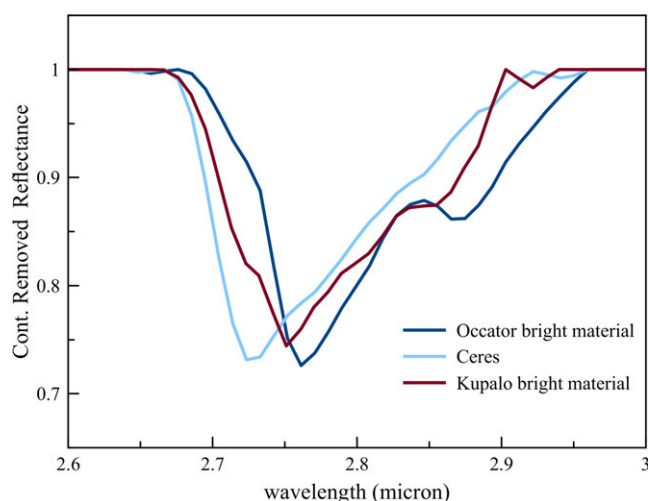

Fig. 8. Continuum-removed spectra of pixels in Occator central dome, Kupalo Crater, and average Ceres. (Color figure can be viewed at wileyonlinelibrary.com.)
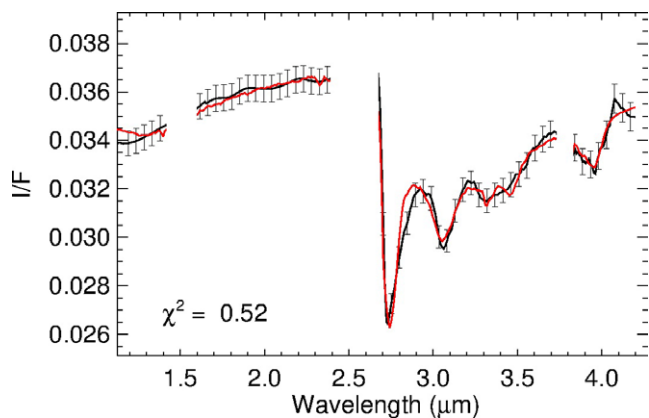

Fig. 9. Spectral fits of the average Ceres spectrum obtained with 9% of ammoniated montmorillonite, 3% of dolomite, 6% of antigorite, 0.05% of brucite, and the remaining part is a the dark neutral component (spectra used in the fit are reported in Table 3 and labeled (2)). (Color figure can be viewed at wileyonlinelibrary.com.)

competes with K^+, which on Earth is more abundant and constitutes a typical component of illite. The laboratory spectra of ammoniated clays often show a signature of adsorbed water caused by the method used for the mineral preparation, making the precise identification of ammoniated phyllosilicate challenging. More laboratory work is needed to identify the ammoniated species responsible for the 3.07 μm band, preparing single minerals and mixtures. Part of this work has been done with brucite mixed with other components, as reported in De Angelis et al. (2016). The spectra of the mixture acquired with the VIR spare (De Angelis et al. 2015) show bands due to the
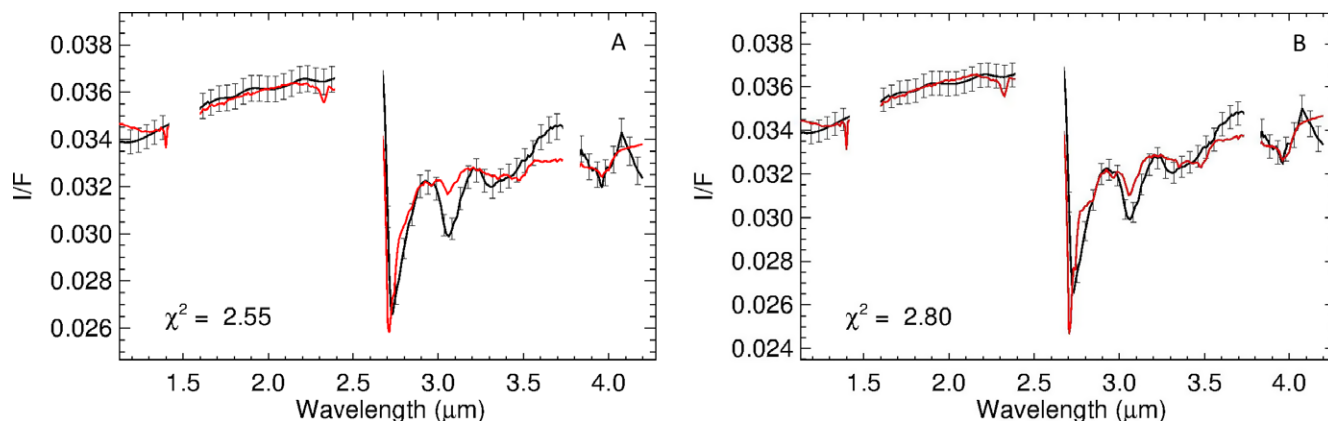
Fig. 10. A) Spectral fit with 5% of brucite. Ceres spectrum has been fitted with the quantity of brucite equal to 5%. The other components used in the mixture are dolomite (3.6%) and antigorite (6.6%). The remaining component is a neutral, dark component similar to magnetite. B) Fit with 10% of brucite. Ceres spectrum has been fitted taking the quantity of brucite equal to 10%. The other components used in the mixture are dolomite (~2%) and antigorite (3.5%). The remaining component is a neutral, dark component similar to magnetite. (Color figure can be viewed at wileyonlinelibrary.com.)

presence of brucite that are not seen in the Ceres spectrum.

Ammannito et al. (2016) found that NH_4-bearing phyllosilicates are ubiquitous across the surface of Ceres, but the intensity of the band is variable and broadly correlated with the intensity of the OH-absorption band at large regional scale. However, at smaller spatial scales, there are locations where intensity variations are inversely correlated (e.g., Urvara Crater).

Ammonium on Ceres is mostly in the form of ammoniated phyllosilicate, but NH_4 salts have also been inferred from the spectra of specific locations (De Sanctis et al. 2016; Raponi et al. 2018). The Occator central dome shows a 2.2 μm absorption with a minimum at 2.21 μm in the brightest pixels. This band can be attributed to NH_4^+-bearing minerals, in particular, NH_4Cl and NH_4CO_3, that show bands at ~2.21 μm (Berg et al. 2016).

Carbonates

The average spectrum of Ceres shows carbonate absorption bands at 3.3–3.6 and 3.9–4 μm. Even if the band is relatively broad, it is possible to discard some kind of carbonate using the spectral modeling to fit the overall spectrum of Ceres (De Sanctis et al. 2015). The results obtained using magnesite and dolomite are the best, but it is difficult to discriminate among the two. Other carbonates, as siderite and calcite, are less likely, according to the results of the spectral fits reported in De Sanctis et al. (2015). In fact, calcite and siderite have band centers at longer wavelengths.

The global distribution of carbonates on Ceres has been mapped using the diagnostic absorption feature in

the 3.95–4.1 μm spectral range. In fact, several different absorptions can contribute to the broad absorption present in the spectral domain between 3.3 and 3.6 μm. For this reason, Carrozzo et al. (2018) preferred to use only the 3.95–4.1 μm spectral range. Carbonate minerals are ubiquitous across the surface, but differences in the strength and position of the absorption features point to variations in both their relative abundance and composition. Most of the surface is compatible with Mg, Ca-carbonates, but confined areas show the presence of Na-carbonates (Fig. 11). Some bright regions, most prominently in Occator Crater, contain deposits of natrite Na_2CO_3 (De Sanctis et al. 2016; Carrozzo et al. 2018). In Occator, the Na-carbonate (45–80 vol%) is mixed with Al-phyllosilicates or with other ammoniated species (carbonate or chloride). Sodium carbonate is also detected on the flanks of Ahuna Mons (Zambon et al. 2017), likely a cryovolcanic dome (Ruesch et al. 2016).

Carrozzo et al. (2018) mapped many other occurrences of Na-carbonates on Ceres, such as in the Kupalo Crater, as also reported by De Sanctis et al. (2017a). Their uneven distribution is indicative of the widespread presence of Na-carbonate below Ceres's surface, although its abundance is heterogeneous. In addition, hydrated Na-carbonate ($Na_2CO_3 \cdot H_2O$) has been identified on a very few localized areas on Ceres (Carrozzo et al. 2018).

Natrite (Na_2CO_3) in the Occator Crater has been interpreted as the result of geologically recent hydrothermal activity (De Sanctis et al. 2016; Raponi et al. 2018; Zolotov and Mironenko 2017). The current estimated age of Occator Crater formation is less than 50 Myr (Neesemann et al. 2017), but the estimated age
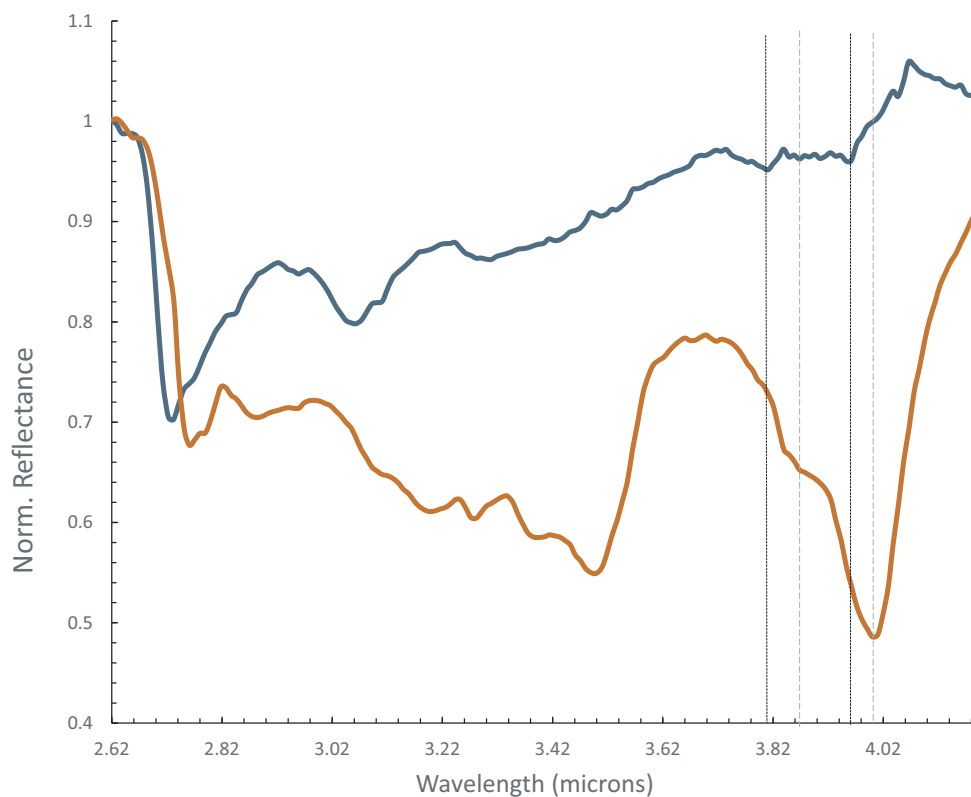
Fig. 11. Representative spectra of Na-carbonate (orange) and (Ca, Mg)-carbonate (blue) rich areas taken from different regions on Ceres. Orange spectrum is an average of Occator bright material taken from VIR_IR_1B_1_494253260_1 (average of 4×4 pixels centered on 70, 19). Blue is taken from an average of 10×10 pixels centered on 56, 22 of cube VIR_IR_1B_1_495269326_1. Vertical lines are used to highlight the different band minima around 3.9–4 µm for both the spectra. (Color figure can be viewed at wileyonlinelibrary.com.)

of the bright deposit is ~5 Myr, which is younger than the age of the crater floor and ejecta. However, there is much uncertainty in the estimated age of the deposit compared with the crater floor ages. Also, the presence of $NaHCO_3$ (Carrozzo et al. 2018), a Na-carbonate that is not stable in the hydrated form on Ceres (Zolotov and Mironenko 2017), indicates that its formation or exposure on Ceres surface is "recent," and dehydration to the anhydrous form Na_2CO_3 is still ongoing.

Water Ice

Water ice was predicted to be unstable at low latitudes on Ceres, but stable at polar sites (Fanale and Salvail 1989; Formisano et al. 2016). Nevertheless, water ice has been discovered locally exposed in nonpolar regions at the surface of Ceres, often associated with very young craters. Several locations exhibit diagnostic absorption bands of the H_2O molecule, notably Oxo and Juling Craters (Combe et al. 2016; Raponi et al. 2017b). The spectra are consistent with water ice mixed with the material that composes

the Cerean surface. The spectrum of an ice-rich pixel in the Oxo Crater is given in Fig. 12. Water ice bands are clearly visible at 1.25, 1.5, 2.0, and 3 µm. Spectral modeling of the icy area in Oxo gives a water ice abundance of up to 15% (Raponi et al. 2017a). The area in Oxo having ice mixed with other materials is approximately 0.15–0.25 km^2.

The observed H_2O exposures are in fresh craters (Combe et al. 2017), mainly at high latitudes. Most of the occurrences are in the northern hemisphere, suggesting a dissimilar abundance of water ice between the north and south polar regions. The global map of hydrogen abundance by GRaND indicates a strong variation with latitude and is asymmetric, with higher water-equivalent hydrogen in the north than in the south (Prettyman et al. 2016), consistent with the exposures of ice in the northern hemisphere. According to the GRaND results and modeling, water ice approaches the surface above 40° latitude in both hemispheres. The VIR data of exposed ice on the surface provide support for this conclusion. The water ice is often found near rim shadows, suggesting that the
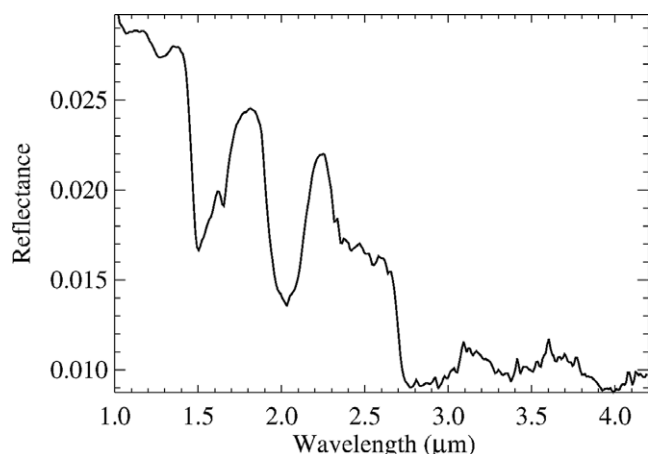
Fig. 12. Spectrum of a water-rich pixel in Oxo crater, obtained during LAMO at a resolution of ~100 m/px. The water ice bands at 1.25, 1.5, 2.0, and 3 microns are clearly visible.

ice is preserved at that specific location on the surface due to the low insolation and very cold environment.

Organic Matter

Searching for organic bands globally across Ceres is hampered by the fact that the 3.2–3.5 μm spectral region partially overlaps the bands for ammoniated phyllosilicate and carbonate minerals. However, localized concentrations of organic matter have been found in and around the Ernutet Crater (De Sanctis et al. 2017b) by analyzing the shape of the ~3.4 μm spectral feature (Fig. 13). The organic-rich area is large, extending for about 1000 km². Another much smaller occurrence was identified in the Inamahari Crater. This area is about 400 km away from Ernutet, so the source for the organics in these two regions must be distinct.

Organic-rich areas near Ernutet also often exhibit other differences relative to the average Ceres surface. Variations in the depth of a carbonate band at 3.9 μm indicate an enhancement of carbonate along the south-west Ernutet rim and perhaps ejecta, although other organic-rich areas in Ernutet do not show any carbonate enhancement (De Sanctis et al. 2017b). Similarly, the distribution of the ammoniated species suggests an increase of this component, possibly correlated with organic-rich areas in Ernutet.

The Ceres band at 3.3–3.5 μm shows marked similarities with the organic bands of terrestrial hydrocarbons, like asphaltite and kerite, considered to be analogs for asteroidal and cometary organics (Moroz et al. 1998). The band is also very similar to the 3.4 μm feature observed in insoluble organic matter (IOM) extracted from the carbonaceous chondrites (Alexander et al. 2007).
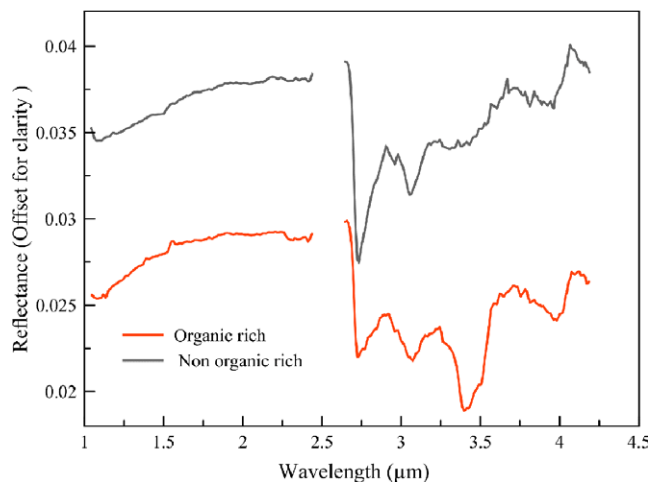

Fig. 13. Comparison between the spectrum of an organic-rich region in Ernutet and the spectrum of the background material. The orange spectrum is an average of seven pixels in Ernutet Crater; the blue spectrum is an average of 25 pixels taken from cube VIR_IR_1B_1_498325369_1. (Color figure can be viewed at wileyonlinelibrary.com.)

The amount of organics in Ernutet can be estimated using a nonlinear mixing algorithm (Hapke modeling), as described in De Sanctis et al. (2017b). The best fits are obtained by an intimate mixture of ~4–9% of hydrocarbons (kerite) with typical background Ceres material (De Sanctis et al. 2017b).

The overall characteristics of the 3.3–3.5 μm band (shape, position, intensity) discovered on Ceres unambiguously indicate the presence of organic material. This material has two possible origins: delivery of foreign organic material from an exogenous source or an endogenous source (De Sanctis et al. 2017b; Pieters et al. 2017). Both hypotheses have pros and cons and are still under debate. Much of the concentration of organic material is associated with very small impact craters, and the observed pattern could be consistent with a field of secondary impacts, but no appropriate primary crater has been found. At the same time, there is also a diffuse weaker background of organic materials. Moreover, organic-rich areas are associated with enhancement of carbonates and ammoniated materials that are typical of Ceres's hydrothermal environment. Finally, the retrieved abundance of organics in Ernutet is relatively high, larger than the abundance in CC, favoring an endogenic origin of the organics on Ceres.

IMPLICATIONS FOR THE ORIGIN OF CERES FROM THE OBSERVED MINERALOGY

Data gathered by the Dawn mission show a dwarf planet where mineralogy and geology were dominated

by the action of water and other volatile ices mixed with rocks. The surface displays clearly the products of aqueous alteration and also ice on the surface (De Sanctis et al. 2015; Ammannito et al. 2016; Combe et al. 2016; Platz et al. 2016). Water ice is present in the immediate subsurface with increasing content toward the polar regions (Prettyman et al. 2016). The surface morphology indicates the presence of recent cryogenic domes and glacial flows (Ruesch et al. 2016; Schmidt et al. 2017). Thus, Ceres has been strongly affected by water-driven processes, some of which are likely active today or in the recent past (De Sanctis et al. 2016).

The presence of ammonia in phyllosilicates and salts (King et al. 1992; De Sanctis et al. 2015, 2016) indicates the accretion of volatiles, such as ammonia and possibly CO_2 and CO ices in the original material from which Ceres formed. The surface shows some similarities with some carbonaceous chondrites (McSween et al. 2017), even if those meteorites do not show ammoniated phyllosilicates and Na-carbonates, as observed on Ceres's surface. The differences can be partially explained by a different level of alteration of Ceres related to the larger size of the body (McSween et al. 2017). In fact, ammonia was found incorporated in the insoluble organic matter of a few carbonaceous chondrites, and it was released upon hydrothermal treatment at 300 °C and 100 MPa (Pizzarello and Williams 2012). Ammonia release was particularly abundant in some CR2 meteorites (Pizzarello and Williams 2012). The data suggest that ammonia was pervasive in the precursor environments where CR2 materials formed, and it is the most abundant single volatile component of these meteorites, pointing to a very cold formation environment, likely different with respect to the main belt.

Ammonia ice is highly volatile and easily sublimates at Ceres's current location. One possibility is that ammonia ice was incorporated into Ceres as it accreted further out in the solar system, as suggested by McKinnon (2012), or as Ceres accreted in its present position while incorporating pebbles from the outer solar system (De Sanctis et al. 2015). In the first hypothesis, Ceres formed in Pluto's neighborhood but later migrated inward under the gravitational pull of Uranus and Neptune. The Nice Model predicts that objects that formed beyond Neptune could have been transported to the inner solar system in large numbers (Levison et al. 2009). This model could explain the observed mixing of asteroid composition in the main belt by implantation of outer solar system material into the asteroid belt (Walsh et al. 2011). Pebble accretion—the process by which planetesimals can grow via the accretion of small, rapidly drifting submeter-sized bodies (Lambrechts and Johansen 2012; Levison et al.

2015)—offers an alternative model without requiring a dramatic migration of the giant planets. In these models, planetesimals from the Jupiter-formation zone can be implanted into the outer main belt via interactions with scattered Jupiter-zone protoplanets, providing a viable alternative to the origin of Ceres (Kretke et al. 2016). A third alternative, advocated by McSween et al. (2017), is that Ceres formed near its present location as an especially large carbonaceous chondrite parent body, with ammonia-bearing organics that were released by advanced thermal alteration.

The observed local mineralogy shares many commonalities with some satellites in the outer solar system, such as Enceladus, which may provide a clue as to the original environment in which Ceres formed. Analyzed plumes erupting from Enceladus contain water, ammonia, and sodium salts, such as NaCl, $NaHCO_3$, and/or Na_2CO_3 as significant constituents (Postberg et al. 2009, 2011). All these chemical species, except for NaCl that is mainly featureless in the VIR spectral range, have been found on Ceres's surface, suggesting a similar composition of the "Cerean liquid" with the "Enceladus liquids." The present location of the two bodies is obviously different, but the similarities in the composition of the minerals suggest similar original compositions and conditions.

Editorial Handling—Dr. Michael Toplis

REFERENCES

A'Hearn M. F. and Feldman P. D. 1992. Water vaporization on Ceres. *Icarus* 98:54–60.
Alexander C. M. O'D., Fogel M., Yabuta H., and Cody G. D. 2007. The origin and evolution of chondrites recorded in the elemental and isotopic compositions of their macromolecular organic matter. *Geochimica et Cosmochimica Acta* 71:4380–4403.
Ammannito E., De Sanctis M. C., Ciarniello M., Frigeri A., Carrozzo F. G., Combe J.-P., Ehlmann B. L., Marchi S., McSween H. Y., Raponi A., Toplis M. J., Tosi F., Castillo-Rogez J. C., Capaccioni F., Capria M. T., Fonte S., Giardino M., Jaumann R., Longobardo A., Joy S. P., Magni G., McCord T. B., McFadden L. A., Palomba E.,

Pieters C. M., Polansky C. A., Rayman M. D., Raymond C. A., Schenk P., Zambon F., Russell C. T., and the Dawn Science Team. 2016. The distribution of phyllosilicates on the surface of Ceres. *Science* 353:1006. https://doi.org/10.1126/science.aaf4279.

Beran A. 2002. Infrared spectroscopy of micas. In *Micas: Crystal chemistry and metamorphic petrology*, edited by Mottana A., Sassi F. P., Thompson J. B., and Guggenheim S. Washington, D.C.: Mineralogical Society of America. pp. 351–370.

Berg B. L., Cloutis E. A., Beck P., Vernazza P., Bishop J. L., Driss T., Reddy V., Applin D., and Mann P. 2016. Reflectance spectroscopy (0.35-8 μm) of ammonium-bearing minerals and qualitative comparison to Ceres-like asteroid. *Icarus* 265:218–237.

Bishop J. L., Banin A., Mancinelli R. L., and Klovstad M. R. 2002. Detection of soluble and fixed NH_4^+ in clay minerals by DTA and IR reflectance spectroscopy: A potential tool for planetary surface exploration. *Planetary and Space Science* 50:11–19.

Bishop J. L., Lane M. D., Dyar M. D., and Brown A. J. 2008. Reflectance and emission spectroscopy study of four groups of phyllosilicates: Smectites, kaolinite-serpentines, chlorites and micas. *Clay Minerals* 43. https://doi.org/10.1180/claymin.2008.043.1.03, 2008.

Carrozzo F. G., Raponi A., De Sanctis M. C., Ammannito E., Giardino M., D'Aversa E., Fonte S., and Tosi F. 2016. Artifacts reduction in VIR/Dawn data. *Reviews of Scientific Instrumentation* 87:124,501. https://doi.org/10.1063/1.4972256.

Carrozzo F. G., De Sanctis M. C., Raponi A., Ammannito E., Castillo-Rogez J., Ciarniello M., Ehlmann B. L., Fonte S., Formisano M., Frigeri A., Giardino M., Magni G., Palomba E., Tosi F., Stains N., Zambon F., Raymond C. A., and Russell C. T. 2018. Distribution of carbonates on Ceres. *Science Advances* 4:e1701645. https://doi.org/10.1126/sciadv.1701645.

Carry B., Dumas C., Fulchignoni M., Merline W. J., Berthier J., Hestroffer D., Fusco T., and Tamblyn P. 2008. Near-infrared mapping and physical properties of the dwarf-planet Ceres. *Astronomy & Astrophysics* 478:235–244.

Castillo-Rogez J., Neveu M., McSween H., Fu R., Toplis M. and Prettyman T. 2018. Insights into Ceres' evolution from surface composition. *Meteoritics & Planetary Science*. Forthcoming.

Ciarniello M., De Sanctis M. C., Ammannito E., Raponi A., Longobardo A., Palomba E., Carrozzo F. G., Tosi F., Li J-Y., Schröder S. E., Zambon F., Frigeri A., Fonte S., Giardino M., Pieters C. M., Raymond C. A., and Russell C. T. 2017. Spectrophotometric properties of dwarf planet Ceres from the VIR spectrometer on board the Dawn mission. *Astronomy & Astrophysics* 598:A130.

Combe J.-P., McCord T. B., Tosi F., Ammannito E., Carrozzo F. G., De Sanctis M. C., Raponi A., Byrne S., Landis M., Hughson K. H. G., Raymond C. A., and Russell C. T. 2016. Detection of local H_2O exposed at the surface of Ceres. *Science* 353:aaf3010. https://doi.org/10.1126/science.aaf3010.

Combe J.-P., Raponi A., McCord T. B., Tosi F., De Sanctis M. C., Ammannito E., Byrne S., Carrozzo F. G., Carsenty U., Hayne P. O., Hughson K. H. G., Johnson K. E., Landis M. E., Pieters C. M., Mazarico E., Platz T., Ruesch O., Schröder S., Singh S. M., Zambon F., Raymond C. A., and Russell C. T. 2017. Exposed H_2O-rich areas detected on Ceres with the Dawn Visible and InfraRed mapping spectrometer. *Icarus*. https://doi.org/10.1016/j.icarus.2017.12.008.

Coradini A., Capaccioni F., Drossart P., Semery A., Arnold G., Schade U., Angrilli F., Barucci M. A., Bellucci G., Bianchini G., Bibring J. P., Blanco A., Blecka M., Bockelee-Morvan D., Bonsignori R., Bouye M., Bussoletti E., Capria M. T., Carlson R., Carsenty U., Cerroni P., Colangeli L., Combes M., Combi M., Crovisier J., Dami M., De Sanctis M. C., DiLellis A. M., Dotto E., Encrenaz T., Epifani E., Erard S., Espinasse S., Fave A., Federico C., Fink U., Fonti S., Formisano V., Hello Y., Hirsch H., Huntzinger G., Knoll R., Kouach D., Ip W. P., Irwin P., Kachlicki J., Langevin Y., Magni G., McCord T., Mennella V., Michaelis H., Mondello G., Mottola S., Neukum G., Orofino V., Orosei R., Palumbo P., Peter G., Pforte B., Piccioni G., Reess J. M., Ress E., Saggin B., Schmitt B., Stefanovitch D., Stern A., Taylor F., Tiphene D., and Tozzi G. 1998. VIRTIS: An imaging spectrometer for the ROSETTA mission. *Planetary and Space Science* 46:1291–1304.

De Angelis S., Ammannito E., Di Iorio T., De Sanctis M. C., Manzari P. O., Liberati F., Tarchi F., Dami M., Olivieri M., Pompei C., and Mugnuolo R. 2015. The spectral imaging facility: Setup characterization. *Review of Scientific Instruments* 86:093,101. https://doi.org/10.1063/1.4929433.

De Angelis S., Manzari P., De Sanctis M. C., Ammannito E., and Di Iorio T. 2016. VIS-IR study of brucite–clay–carbonate mixtures: Implications for Ceres surface composition. *Icarus* 280:315–327.

De Sanctis M. C., Coradini A., Ammannito E., Filacchione G., Capria T., Fonte S., Magni G., Barbis A., Vini A., Dami M., Fical-Veltroni I., Preti G., and the VIR Team. 2011. The VIR spectrometer. *Space Science Reviews* 163:329–369.

De Sanctis M. C., Ammannito E., Raponi A., Marchi S., McCord T. B., McSween H. Y., Capaccioni F., Capria M. T., Carrozzo F. G., Ciarniello M., Longobardo A., Tosi F., Fonte S., Formisano M., Frigeri A., Giardino M., Magni G., Palomba E., Turrini D., Zambon F., Combe J.-P., Feldman W., Jaumann R., McFadden L. A., Pieters C. M., Prettyman T., Raymond C. A., and Russell C. T. 2015. Ammoniated phyllosilicates with a likely outer solar system origin on (1) Ceres. *Nature* 528:241–244.

De Sanctis M. C., Raponi A., Ammannito E., Ciarniello M., Toplis M. J., McSween H. Y., Castillo-Rogez J. C., Ehlmann B. L., Carrozzo F. G., Marchi S., Tosi F., Zambon F., Capaccioni F., Capria M. T., Fonte S., Formisano M., Frigeri A., Giardino M., Longobardo A., Magni G., Palomba E., McFadden L. A., Pieters C. M., Jaumann R., Schenk P., Mugnuolo R., Raymond C. A., and Russell C. T. 2016. Bright carbonate deposits as evidence of aqueous alteration on (1) Ceres. *Nature* 536:54–57. https://doi.org/10.1038/nature18290.

De Sanctis M. C., Ammannito E., Carrozzo G., Ciarneillo M., Frigeri A., Raponi A., Tosi F., Zambon F., Raymond C. A., and Russell C. T. 2017a. Ac-11-Sintana and Ac-H-12 Toharu quadrangles: Assessing the large and small scale heterogeneities of Ceres' surface. *Icarus*. https://doi.org/10.1016/j.icarus.2017.08.014.

De Sanctis M. C., Ammannito E., McSween H. Y., Raponi A., Marchi S., Capaccioni F., Capria M. T., Carrozzo G., Ciarneillo M., Fonte S., Formisano M., Frigeri A.,

Giardino M., Longobardo A., Magni G., McFadden L. A., Palomba E., Pieters C. M., Tosi F., Zambon F., Raymond C. A., and Russell C. T. 2017b. Localized aliphatic organic material on the surface of Ceres. *Science* 355:719–722.

Ehlmann B. L., Hodyss R., Ammannito E., Rossman G. R., De Sanctis M. C., and Raymond C. A. 2018. Ammoniation of phyllosilicates, carbonaceous chondrite meteorites, and implication for the nature of ammoniated materials on Ceres. *Meteoritics & Planetary Science*. 2018, https://doi.org/10.1111/maps.13103.

Fanale F. P. and Salvail J. R. 1989. The water regime of asteroid (1) Ceres. *Icarus* 82:97–110.

Farmer V. C. 1974. The layer silicates. In *The infrared spectra of minerals*, Monograph 4, edited by Farmer V. C. London: Mineralogical Society. pp. 331–363.

Feierberg M. A., Lebofsky L. A., and Larson H. P. 1981. Spectroscopic evidence for aqueous alteration products on the surfaces of low-albedo asteroids. *Geochimica et Cosmochimica Acta* 45:971–981.

Formisano M., De Sanctis M. C., Magni G., Federico C., and Capria M. T. 2016. Ceres water regime: Surface temperature, water sublimation and transient exo (atmo)sphere. *Monthly Notices of the Royal Astronomical Society* 455:1892–1904.

King T. V. V. and Clark R. N. 1989. Spectral characteristics of chlorites and Mg-serpentines using high resolution reflectance spectroscopy. *Journal of Geophysical Research* 94:13,997–14,008.

King T. V., Clark R. N., Calvin W. M., Sherman D. M., and Brown R. H. 1992. Evidence for ammonium-bearing minerals on Ceres. *Science* 255:1551–1553.

Kretke K. A., Levison H. F., and Bottke W. 2016. Exploring how giant planet formation affected the Asteroid Belt. Division of Planetary Sciences. American Astronomical Society, #48, id.518.03

Kueppers M., O'Rourke L., Bodkelee-Morvan D., Zakharov V., Lee S., von Allmen P., Carry B., Teyssier D., Marston A., Muller T., Crovisier J., Barucci M. A., and Moreno R. 2014. Localized sources of water vapour on the dwarf planet (1) Ceres. *Nature* 505:525–527.

Lambrechts M. and Johansen A. 2012. Rapid growth of gas-giant cores by pebble accretion. *Astronomy & Astrophysics* 544:A32.

Lebofsky L. A. 1978. Asteroid 1 Ceres—Evidence for water of hydration. *Monthly Notices of the Royal Astronomical Society* 182:17P–21P.

Lebofsky L. A., Feiererg M. A., Tokunaga A. T., Larson H. P., and Johnson J. R. 1981. The 1.7-4.2-micron spectrum of asteroid 1 Ceres—Evidence for structural water in clay minerals. *Icarus* 48:453–459.

Levison H. F., Bottke W. F., Gounelle M., Morbidelli A., Nesvorný D., and Tsiganis K. 2009. Contamination of the asteroid belt by primordial trans-Neptunian objects. *Nature* 460:364–366.

Levison H. F., Kretke K. A., and Duncan M. J. 2015. Growing the gas-giant planets by the gradual accumulation of pebbles. *Nature* 524:322–324.

Li J.-Y., McFadden L. A., Parker J. W., Young E. F., Stern A. S., Thomas P. C., Russell C. T., and Sykes M. V. 2006. Photometric analysis of 1 Ceres and surface mapping from HST observations. *Icarus* 182:143–160.

McCord T. B. and Castillo Rogez J. C. 2018. Ceres evolution: Before and after the Dawn mission. *Meteoritics & Planetary Science*. Forthcoming.

McKinnon W. B. 2012. Where did Ceres accrete? *Asteroids, Comets, Meteors*. LPI Contribution 1667. Houston, Texas: Lunar and Planetary Institute. p. 6475.

McSween H., Emery J. P., Rivkin A. S., Toplis M. J., Castillo-Rogez J., Prettyman T. H., De Scantis M. C., Pieters C. M., Raymond C. A., and Russell C. T. 2017. Carbonaceous chondrites as analogs for the composition and alteration of Ceres. *Meteoritics & Planetary Science*. https://doi.org/10.1111/maps.12947.

Milliken R. E. and Rivkin A. S. 2009. Brucite and carbonate assemblages from altered olivine-rich materials on Ceres. *Nature Geoscience* 2:258–261.

Moroz L. V., Arnold G., Korochantsev A. V., and Wasch R. 1998. Natural solid bitumens as possible analogs for cometary and asteroid organics. *Icarus* 134:253–268.

Neesemann A., Van Gasselt S., Schmedemann N., Marchi S., Walter S. H. G., Preusker F., Michael G. G., Kneissl T., Hiesinger H., Jaumann R., Roatsch T., Raymond C. A., and Russell C. T. 2017. The various ages of Occator crater, Ceres: Results of a comprehensive synthesis approach. *To appear in Icarus*.

Pieters C. M., Nathues A., Thangiam G., Hoffmann M., Platz T., De Sanctis M. C., Ammannito E., Tosi F., Zambon F., Pasckert J. H., Hiesinger H., Schröder S. E., Jaumann R., Matz K.-D., Castillo-Rogez J. C., Ruesch O., McFadden L. A., O'Brien D. P., Sykes M., Raymond C. A., and Russell C. T. 2017. Geologic constraints on the origin of red organic-rich material on Ceres. *Meteoritics & Planetary Science*. https://doi.org/10.1111/maps.13008.

Pizzarello S. and Williams L. B. 2012. Ammonia in the early solar system: An account from carbonaceous meteorites. *The Astrophysical Journal* 749:161–167.

Platz T., Nathues A., Schorghofer N., Preusker F., Mazarico E., Schröder S. E., Byrne S., Kneissl T., Schmedemann N., Combe J.-P., Schäfer M., Thangjam G. S., Hoffmann M., Gutierrez-Marques P., Landis M. E., Dietrich W., Ripken J., Matz K.-D., and Russell C. T. 2016. Surface water-ice deposits in the northern shadowed regions of Ceres. *Nature Astronomy* 1:0007. https://doi.org/10.1038/s41550-016-0007.

Postberg F., Kempf S., Schmidt J., Brilliantov N., Beinsen A., Abel B., Buck U., and Srama R. 2009. Sodium salts in E ring ice grains from an ocean below the surface of Enceladus. *Nature* 459:1098–1101.

Postberg F., Schmidt J., Hillier J., Kempf S., and Srama R. 2011. A salt-water reservoir as the source of a compositionally stratified plume on Enceladus. *Nature* 474:620–622.

Prettyman T. H., Feldman W., McSween H. Y., Dingler R., Enemark D., Patrick D., Storms S., Hendricks J., Morgenthaler J., Pitman K., and Reedy R. 2011. Dawn's gamma ray and neutron detector. *Space Science Reviews* 163:371–459.

Prettyman T. H., Yamashita N., Toplis M. J., McSween H. Y., Schorghofer N., Marchi S., Feldman W. C., Castillo-Rogez J., Forni O., Lawrence D. J., Ammannito E., Ehlmann B. L., Sizemore H. G., Joy S. P., Polanskey C. A., Rayman M. D., Raymond C. A., and Russell C. T. 2016. Extensive water ice within Ceres' aqueously altered regolith: Evidence from nuclear spectroscopy. *Science* 355:55–59.

Raponi A., Carrozzo F. G., Zambon F., De Sanctis M. C., Ciarniello M., Frigeri A., Ammannito E., Tosi F., Combe J.-P., Longobardo A., Palomba E., Pieters C. M.,

Raymond C. A., and Russell C. T. 2017a. Mineralogical mapping of Coniraya Quadrangle of the Dwarf Planet Ceres. *Icarus*. https://doi.org/10.1016/j.icarus.2017.10.023.

Raponi A., De Sanctis M. C., Frigeri A., Ammannito E., Ciarniello M., Formisano M., Combe J.-P., Magni G., Tosi F., Carrozzo F. G., Fonte S., Giardino M., Joy S. P., Polanskey C., Rayman M. D., Capaccioni F., Capria M. T., Longobardo A., Palomba E., Zambon F., Raymond C. A., and Russell C. T. 2017b. Variations in the amount of water ice on Ceres' surface suggest a seasonal water cycle. *Science Advances* 4:eaao3757. https://doi.org/10.1126/sciadv.aao3757.

Raponi A., De Sanctis M. C., Carrozzo F. G., Ciarniello M., Castillo-Rogez J. C., Ammannito E., Frigeri A., Longobardo A., Palomba E., Tosi F., Zambon F., Raymond C. A., and Russell C. T. 2018. Mineralogy of Occator Crater on Ceres. *Icarus*. https://doi.org/10.1016/j.icarus.2018.02.001.

Reininger F. M., Coradini A., Capaccioni F., Capria M. T., Cerroni P., De Sanctis M. C., Magni G., Drossart P., Barucci M. A., Bockelee-Morvan D., Combes J.-M., Crovisier J., Encrenaz T., Reess J.-M., Semery A., Tiphene D., Arnold G., Carsenty U., Michaelis H., Mottola S., Neukum G., Peters G., Schade U., Taylor F. W., Calcutt S. B., Vellacott T., Venters P., Watkins R. E., Bellucci G., Formisano V., Angrilli F., Bianchini F., Saggin B., Bussoletti E., Colangeli L, Mennella V., Fonti S., Bibring J.-P., Langevin Y, Schmitt B., Combi M., Fink U., McCord T. B., Ip W., Carlson R. W., and Jennings D. E. 1996. VIRTIS: Visible Infrared Thermal Imaging Spectrometer for the Rosetta mission. In *Imaging spectrometry II*, edited by Descour M. R. and Mooney J. M. *Proceedings SPIE* 2819:66–77.

Rivkin A. S. and Volquardsen E. L. 2009. Rotationally-resolved spectra of Ceres in the 3-µm region. *Icarus* 206:327–333.

Rivkin A. S., McFadden L. A., Binzel R. P., and Sykes M. 2006a. Rotationally-resolved spectroscopy of Vesta I: 2–4 µm region. *Icarus* 180:464–472.

Rivkin A. S., Volquardsen E. L., and Clark B. E. 2006b. The surface composition of Ceres: Discovery of carbonates and iron-rich clays. *Icarus* 185:563–567.

Rousselot P., Jehin E., Manfroid J., Mousis O., Dumas C., Carry B., Marboeuf U., and Zucconi J.-M. 2011. Search for water vaporization on Ceres. *Astronomical Journal* 142:125.

Ruesch O., Platz T., Schenk P., McFadden L. A., Castillo-Rogez J. C., Quick L. C., Byrne S., Preusker F., O'Brien D. P., Schmedemann N., Williams D. A., Li J.-Y., Bland M. T., Hiesinger H., Kneissl T., Neesemann A., Schaefer M., Pasckert J. H., Schmidt B. E., Buczkowski D. L., Sykes M. V., Nathues A., Roatsch T., Hoffmann M., Raymond C. A., and Russell C. T. 2016. Cryovolcanism on Ceres. *Science* 353:1005.

Russell C. T. and Raymond C. A. 2011. The dawn mission to Vesta and Ceres. *Space Science Reviews* 163:3–23.

Russell C. T., Raymond C. A., Ammannito E., Buczkowski D. L., De Sanctis M. C., Hiesinger H., Jaumann R., Konopliv A. S., McSween H. Y., Nathues A., Park R. S., Pieters C. M., Prettyman T. H., McCord T. B., McFadden L. A., Mottola S., Zuber M. T., Joy S. P., Polanskey C., Rayman M. D., Castillo-Rogez J. C., Chi P. J., Combe J.-P., Ermakov A., Fu R. R., Hoffman M., Jia Y. D., King S. D., Lawrence D. J., Li J.-Y., Marchi S., Preusker F., Roatsch T., Ruesch O., Schenk P., Villarreal M. N., and Yamashita N. 2016. Dawn arrives at Ceres: Exploration of a small, volatile-rich world. *Science* 353:1008–1010.

Schmidt B., Hughson K., Chilton H., Scully J., Platz T., Nathues A., Sizemore H., Bland M., Byrne S., Marchi S., O'Brien D., Schorghofer N., Hiesinger H., Jaumann R., Pasckert H., Lawrence J., Buczkowski D., Castillo-Rogez J., Sykes M., Schenk P., De Sanctis M. C., Mitri G., Formisano M., Li Y. J., Reddy V., Le Corre L., Russell C. T., and Raymond C. A. 2017. Geomorphological evidence for ground ice on dwarf planet Ceres. *Nature Geoscience* 10:338–343.

Sierks H., Keller H. U., Jaumann R., Michalik H., Behnke T., Bubenhagen F., Büttner I., Carsenty U., Christensen U., Enge R., Fiethe B., Gutiérrez Marqués P., Hartwig H., Krüger H., Kühne W., Maue T., Mottola S., Nathues A., Reiche K.-U., Richards M. L., Roatsch T., Schröder S. E., Szemerey I., and Tschentscher M. 2011. The Dawn framing camera. *Space Science Reviews* 163:263–327.

Takir D., Emery J. P., McSween H. Y., Hibbitts C. A., Clark R. N., Pearson N., and Wang A. 2013. Nature and degree of aqueous alteration in CM and CI carbonaceous chondrites. *Meteoritics & Planetary Science* 48:1618–1637.

Thomas P. C., Parker J. Wm, McFadden L. A., Russell C. T., Stern S. A., Sykes M. V., and Young E. F. 2005. Differentiation of the asteroid Ceres as revealed by its shape. *Nature* 437:224–226.

Vernazza P., Mothé-Diniz T., Barucci M. A., Birlan M., Carvano J. M., Strazzulla G., Fulchignoni M., and Migliorini A. 2005. Analysis of near-IR spectra of 1 Ceres and 4 Vesta, targets of the Dawn mission. *Astronomy & Astrophysics* 436:1113–1121.

Walsh K. J., Morbidelli A., Raymond S. N., O'Brien D. P., and Mandell A. M. 2011. A low mass for Mars from Jupiter's early gas-driven migration. *Nature* 475:206–209.

Zambon F., Raponi A., Rosi F., De Sanctis M. C., McFadden L. A., Carrozzo F. G., Longobardo A., Ciarniello M., Krohn K., Stephan K., Palomba E., Pieters C. M., Ammannito E., Russell C. T., and Raymond C. A. 2017. Spectral analysis of Ahuna Mons from Dawn mission's visible-infrared spectrometer. *Geophysical Research Letters* 44:97–104.

Zolotov M. Y., and Mironenko M. V. 2017. Bright salts on Ceres: aqueous accumulation and airborne emplacement (abstract #1241). 48th Lunar and Planetary Science Conference. CD-ROM.

APPENDIX 1

Data acquired by the VIR spectrometer are systematically affected by artifacts, vertical stripes, and spikes, as describe in Carrozzo et al. (2016), mainly due to imperfect radiometric and spectral on-ground calibration. Carrozzo et al. (2016), after having identified systematic artifacts in the spectra, developed a de-noising algorithm. In particular, the algorithm removes some artifacts in the instrumental response function (IRF) in the NIR-IR spectral range. These artifacts are systematic, and therefore, they do not prevent the detection of relative spectral variations. Nevertheless, in Carrozzo et al.'s (2016) procedure, the
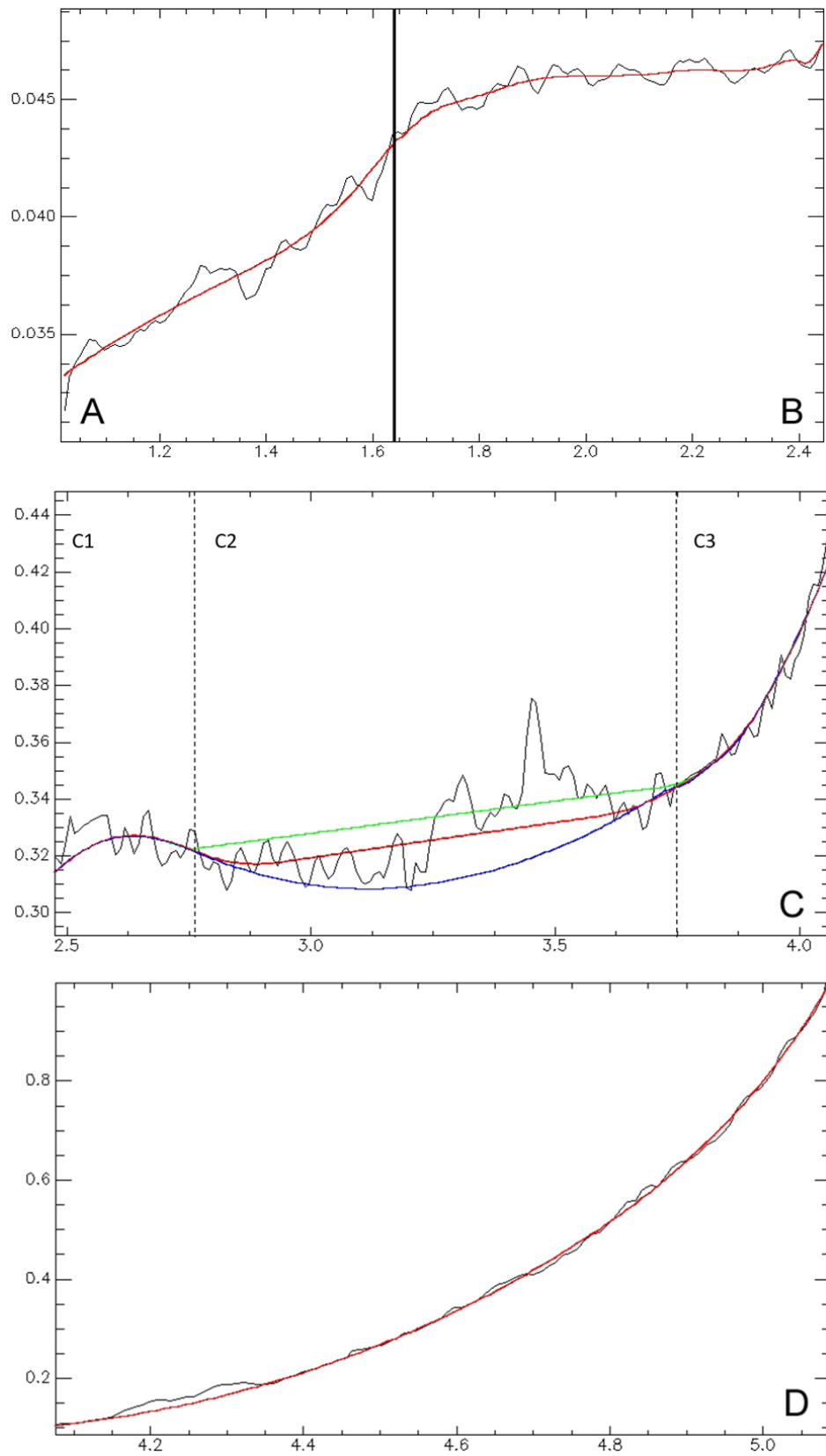
Fig. A1. Ceres and Vesta VIR data (black line) and fitting curve (red line) in the different IR spectral ranges. (Color figure can be viewed at wileyonlinelibrary.com.)
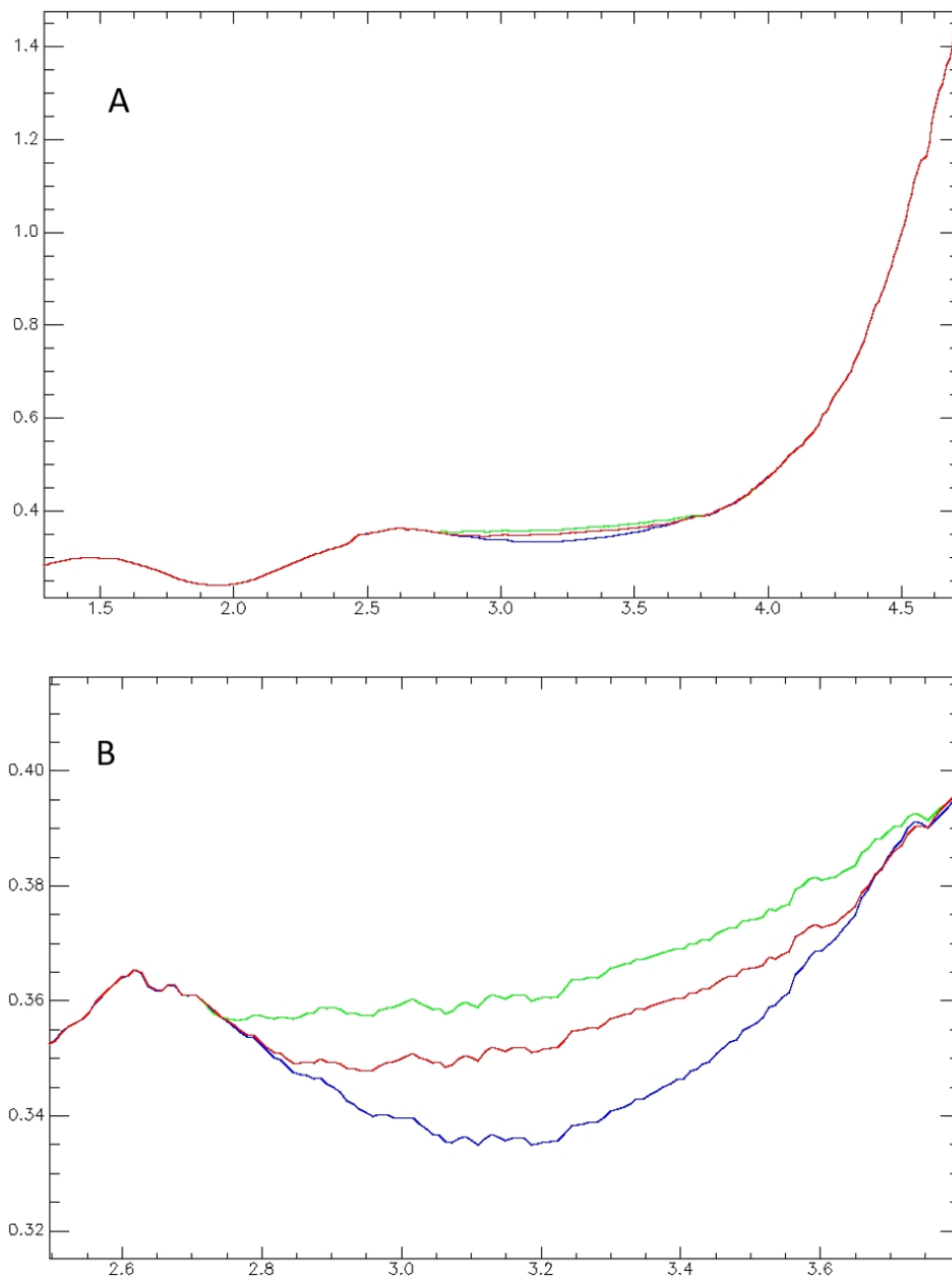
Fig. A2. A) Vesta average spectrum in the IR obtained using the different matrix. B) Zoom in the 2.5–3.75 μm range showing the results obtained using the different matrix. (Color figure can be viewed at wileyonlinelibrary.com.)

uncertainties on the spectra introduced by the de-noise algorithm were not evaluated. Here, we revise the algorithm to evaluate these uncertainties.

The correction of artifacts was made in a two-step process that included the (1) creation of the artifacts matrix and (2) application of the artifacts matrix to the VIR cubes. The first part of step 1 is the creation of a polynomial function to fit the high-frequency variations present in the Vesta and Ceres spectra (Carrozzo et al. 2016). The polynomial functions are created using Ceres or Vesta VIR data in different spectral ranges, subsequently choosing the spectrum of the body which presents weak or absent spectral features in the specific range. Below are the spectral ranges, data, and function for the fitting:
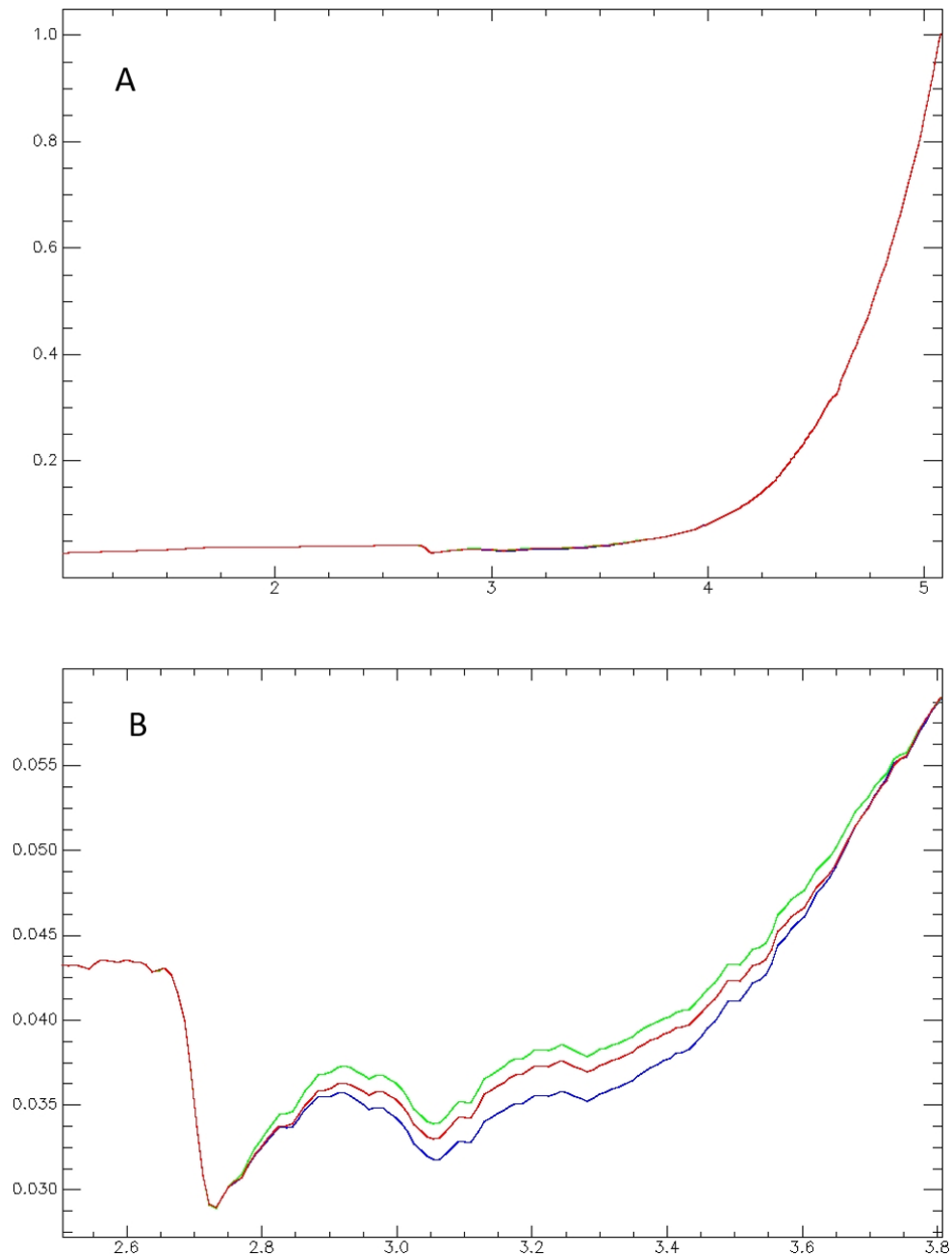
Fig. A3. A) Ceres average spectrum in the IR obtained using the different matrix. B) Zoom in the 2.5–3.75 μm range showing the results obtained using the different matrix. (Color figure can be viewed at wileyonlinelibrary.com.)

Table A1. Polynomial functions in different spectral ranges

	Range (microns)	Data	Function
A	1.0–1.64	Ceres	Polynomial 3°
B	1.64–2.44	Ceres	Smooth box 3
C1	2.44–2.8	Vesta	Polynomial 5°
C2	2.8–3.75	Vesta	Polynomial 2°
C3	3.75–4.06	Vesta	Polynomial 3°
D	4.06–5.2	Ceres	Polynomial 3°

Table A2. Evaluation of spectral parameters evaluation

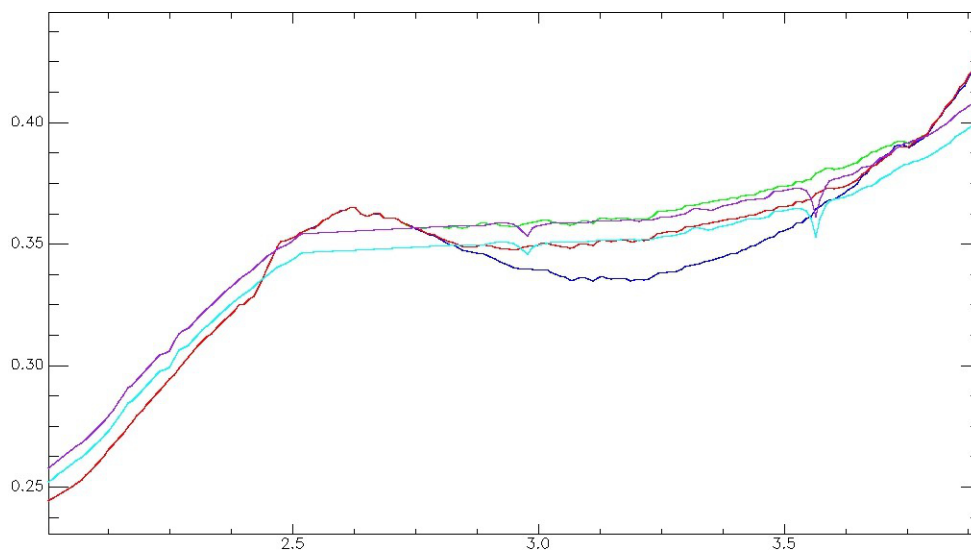| Curve	2.7 band depth	2.7 band center (micron)	3.1 band depth	3.1 band center (micron)
Red	0.22	2.73	0.11	3.06
Green	0.22	2.73	0.12	3.06
Blue	0.24	2.73	0.12	3.07

Fig. A4. Zoom in the 2.5–3.75 μm range showing the results obtained using the different matrix compared with Vesta ground-based spectrum (magenta data are scaled at 2.75 μm, cyan data are scaled at 2.83 μm). (Color figure can be viewed at wileyonlinelibrary.com.)

The fact that the polynomial fit can be computed in different ways is the major source of uncertainties with the de-noised spectra. There are spectral regions (1.64–2.44 μm) where the fitting is quite straightforward because it resembles a simple smoothing of the data. However, the spectral region between 2.8 and 3.7 μm is the most difficult range to fit (Fig. A1). Comparing the ground-based spectrum of Vesta and the data acquired by VIR, we recognize that the VIR data show an excess between 3.25 and 3.65 μm and a deficiency 2.75 and 3.25 μm (Fig. A1). We fit that region with a polynomial curve (red line in Fig. A1).

Table A3. Retrieved abundances using the green matrix and the red matrix.

Matrix	Antigorite (%)	NH$_4$-mont (%)	Dolomite (%)	Dark component (%)	Grain size (μm)
Green	6.8	7.9	2.6	82.7	65
Red	6.9	9.1	2.7	81.3	46

However, different choices can be tested, and here we explore how the results change using different fitting curves in "C2" spectral ranges. We made two extreme choices (1) blue curve, assuming that the entire spectral range in C2 has an excess; (2) green, assuming that most of the spectral range in C2 shows a deficiency (Fig. A1 middle panel). Using these two other curves, we computed two more matrices to be applied to the
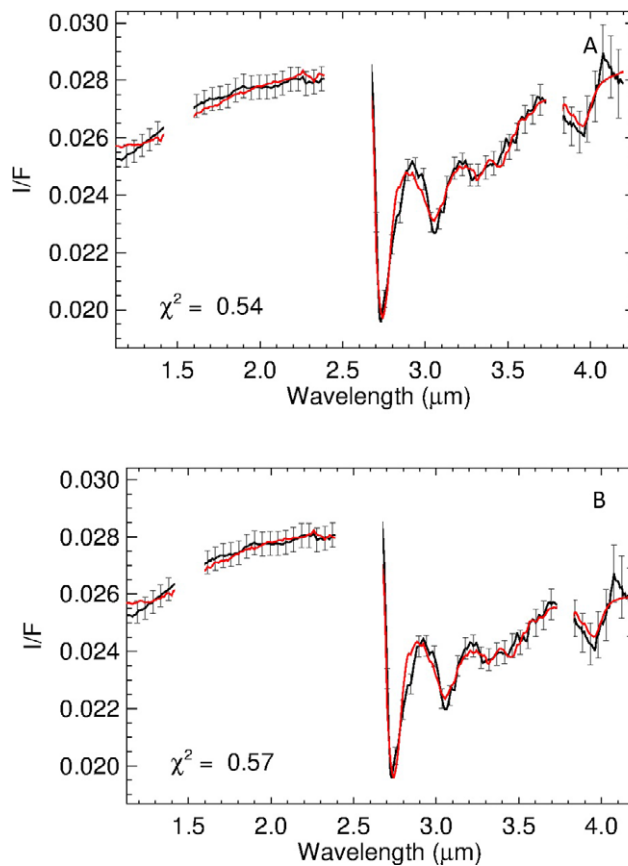

Fig. A5. Spectral fit (red line) of the Ceres average spectrum (black line) obtained with the green matrix (A) and red matrix curve (B). (Color figure can be viewed at wileyonlinelibrary.com.)

data. The resulting average spectra of Ceres and Vesta are in Figs. A2 and A3.

In all the different cases, the overall spectra are very similar to each other, because the different matrices do not create/cancel narrow absorptions in the 2.8–3.7 μm range in the Ceres spectrum.

However, we evaluated the bands characteristics in a quantitative way, computing the Ceres band centers and depths (Table A2). Band centers and depths are computed as explained in Ammannito et al. (2016).

The largest differences are found using the blue curve fit, but the comparison between the ground-based Vesta spectra and the spectra acquired by VIR shows that the blue fitting curve is the one that gives the less reasonable results (Fig. A4).

Figure A4 shows the comparison between ground-based spectra of Vesta taken from Rivkin et al. (2006) and Vesta VIR data obtained using a different matrix. We think that is reasonable to discard the blue fit of the data. Thus, taking into account only the red and green fits, we do not observe significant differences of the respective band parameters.

The evaluation of the abundances in the two cases has been done using the method explained in De Sanctis et al. (2015). The results are reported in Table A3 and Fig. A5 (a—green matrix; b—red matrix).